Privatdoz. Dipl.-Ing. Dr.techn. Andreas Limbeck

TU WIEN
TECHNISCHE
UNIVERSITÄT
WIEN
Vienna University of Technology

Diplomarbeit

LA-ICP-MS analysis of boron additives in PM-steel samples

Ausgeführt am Institut für

Chemische Technologien und Analytik

der Technischen Universität Wien

Unter der Anleitung von

Privatdoz. Dipl.-Ing. Dr.techn Andreas Limbeck

Univ.Ass. Dipl.-Ing. Dr.techn. Christian Gierl-Mayer

durch

Viktor Bauer, BSc.

Mat. Nr. 0825503

Liechtensteinstraße 98/8

1090 Wien

Wien, Mai 2015

Viktor Bauer

"There is only one corner of the universe you can be certain of improving, and that's your own self."

- Aldous Huxley

Abstract

The activated sintering of steels by addition of boron is an attractive method to attain high densities. But still there is the danger of an enrichment of brittle phases on grain boundaries, as the solubility of boron is extremely low which on the other hand is a key factor for the sintering with activating liquid phase. Chromium as an alloying element changes the solubility a little, and therefore the sensitivity against the formation of these brittle phases. Also the sintering atmosphere plays a major role, as boron tends to react with hydrogen and nitrogen. When using argon as an inert sintering gas, the formation of volatile boride compounds is prevented but porosity of the bulk material occurs.

The quantitative analysis of boron is known to be very tricky, as the usual methods such as XRF and SEM-EDS, are not very sensitive because of the low atomic number of boron.

In this work, Laser Ablation -Inductively Coupled Plasma Mass Spectrometry analysis, LA-ICP-MS, is demonstrated on boron containing PM-steels. It is a very sensitive and accurate detection technique which enables measurement of most of the elements and provides high sample throughput. Moreover, for boron there aren't any noticeable interferences with other elements which could disturb the analysis. However, LA-ICP-MS measurement of solid samples requires matrix matched calibration standards since the ablation process is strongly matrix dependent which is also the downside of that instrumental analysis.

The goal was to allow valid and representative quantification of boron in steel samples. The Development of measuring methods or rather the optimization of measurement conditions was a major key point. Also, evaluation of physical and mechanical properties as well as a metallographic examination were carried out to establish a correlation between analytical results and material characteristics.

In the course of this work, the successful set up of a calibration function for the quantification of boron in solid steel-samples could be accomplished by utilizing stock solution for liquid measurements and self-made, vacuum-sintered pellets as standards for solid-sample measurements. Based on that, the total concentration of boron in hydrogen- and argon sintered sample bodies could be quantified.

Investigations show that boron enhances densification in PM-steel samples, forming a liquid eutectic phase which increases diffusion of material during sintering. Low solubility of boron

leads to the formation of a brittle boron-rich phase at grain boundaries, resulting in poor mechanical properties in PM-steels. The imaging of sample cross sections reveals those boron-rich phases and emphasizes a much less uniform distribution of boron in argon sintered samples.

Results for LA-ICP-MS analysis of boron depth-profile show lower normalized boron signals at surface adjacent areas compared to those in the bulk material for hydrogen-sintered samples, suggesting a concentration gradient due to the formation of volatile borides during sintering. Additionally, hydrogen-sintered samples exhibit lower quantities of boron compared to their concentration equivalents which were sintered in argon, when measuring total boron concentration with the LA-ICP-MS.

The optimization of this specific method is far from done, whereby methods enabling the quantification of bulk concentration of boron have successfully been established. Improvements in imaging (lateral quantification) and analysis of depth profile of boron in terms of spatial resolution are primarily limited to the inhomogeneous distribution of boron in investigated solid samples. Therefore, there is a need for enhancements for the fabrication of solid standards in order to improve homogeneity, otherwise purchasing certified standard material should be taken into consideration. Finally, replicates of investigated samples need to be analyzed in order to validate the results and achieve statistical security.

Kurzfassung

Das aktivierte Sintern von pulvermetallurgisch hergestellten Stählen durch die Zugabe von Bor ist eine attraktive Methode, um eine hohe Verdichtung des Materials zu erzielen. Die niedrige Löslichkeit des Bors im Stahl ist die Grundlage dieses Sinterverfahrens, allerdings kann dieser Aspekt auch nachteilig wirken, da es zur Ausscheidung borreicher spröder Phasen an den Korngrenzen des Materials kommen kann. Des Weiteren, ist die Art der Sinteratmosphäre für den Sinterprozess von Bedeutung. Bei Anwendung von Gasen wie Wasserstoff, oder Stickstoff, kommt es zur Bildung flüchtiger Hydroboride bzw. Hydronitride, die den Borgehalt im PM-Stahl maßgeblich verringern können. Um das zu verhindern, kann Argon als Sintergas angewendet werden, wobei es hierbei durch Einschließen des Gases zur Erhöhung der Porosität und damit zu nicht abschätzbaren Verschlechterungen der Materialeigenschaften kommen kann.

Die quantitative Bestimmung von Bor ist eine komplizierte Angelegenheit, da aufgrund seiner niedrigen Ordnungszahl die üblicherweise eingesetzten instrumentellen Analysemethoden, wie das REM-EDX oder RFA, nicht sensitiv genug auf dieses Element reagieren.

In dieser Arbeit soll die Bestimmung des Bors in PM-Stählen mit der Methode der Laser Ablation-induktiv gekoppelten Plasma-Massenspektrometrie (LA-ICP-MS demonstriert werden. Eigenschaften, wie ihre gute Präzision und Empfindlichkeit, genauso wie ihr hoher Probendurchsatz, gehören zu den Vorteilen dieser instrumentellen Analysemethode. Noch dazu, profitiert konkret die Quantifizierung des Bors davon, dass die Methode von Störungen der Messung durch Elementinterferenzen ausgenommen ist. Ein klarer Nachteil ist allerdings, dass diese instrumentelle Messmethode auf Standards angewiesen ist, da Matrixeffekte einen starken Einfluss auf den Probenabtragsprozess und letztendlich auf den Ausgang der Messung haben.

Das formulierte Ziel dieser Arbeit war, eine repräsentative und korrekte Quantifizierung von Bor in pulvermetallurgisch hergestelltem Stahl zu erzielen. Dabei wurde besonderer Fokus auf die Entwicklung einer Messmethode und damit verbunden die Optimierung der Messparameter, gelegt. Zusätzlich galt es die hergestellten Stahlproben auf ihre physikalischen und mechanischen Eigenschaften zu untersuchen sowie eine metallografische Charakterisierung durchzuführen, um letztendlich eine Korrelation zwischen den erhaltenen Werkstoffmerkmalen und den Ergebnissen der analytischen Untersuchung zu erhalten.

Im Zuge dieser Arbeit, wurde eine Kalibrierfunktion zur Quantifizierung von Bor auf Grundlage von zuvor erzeugter, im Vakuum gesinterter Festkörperstandards aufgestellt und deren Konzentration durch wässrigen Aufschluss und nachfolgender Flüssigmessung bestimmt. Dadurch konnte die quantitative Bestimmung des Bors in Argon und Wasserstoff gesinterten Stahlproben gewährleistet werden.

Wie erwartet, zeigen die Untersuchungen, dass die Zugabe von Bor die Bildung einer eutektischen Flüssigphase bewirkt und die Verdichtung des Materials fördert. Weiters, führt die schlechte Löslichkeit des Bors in der Matrix zur Ausbildung einer harten, aber spröden, eutektischen Phase, die sich an den Korngrenzen anlagert, wobei sich bei steigender Konzentration dieses Elements die mechanischen Eigenschaften der PM-Stähle verschlechtern. Mittels eines eigens entwickelten Imaging-Verfahrens konnten die besagten borreichen Ausscheidungen per LA-ICP-MS Analyse festgemacht werden, wobei diese in den mit Argon gesinterten Proben viel ungleichmäßiger verteilt sind, als in den Proben, die mit Wasserstoff behandelt wurden.

Ergebnisse für die normalisierten Borsignale ($^{11}B/^{58}Fe$) aus der Analyse der Tiefenverteilung von Bor in PM-Stahlproben zeigen höhere Analytkonzentrationen an den oberflächennahen Bereichen im Vergleich zum Inneren der Wasserstoff gesinterten Proben auf, was auf einen Konzentrationsgradienten des Bors hindeutet, der durch die Bildung flüchtiger Hydroboride zu begründen ist. Außerdem weisen Messungen der Gesamtkonzentration des Bors mittels LA-ICP-MS auf einen niedrigeren Wert bei Wasserstoff gesinterten Proben hin, verglichen mit der ermittelten Gesamtkonzentration der Proben, die mit Argon gesintert wurden.

Zusammenfassend muss gesagt werden, dass noch einiges an Arbeit geleistet werden muss, um die Analytik des Bors in PM-Stahl mittels LA-ICP-MS zu optimieren. Für die Quantifizierung von Bor im Bulkmaterial wurde die Methodenentwicklung erfolgreich abgeschlossen und eine Kalibrationsfunktion mit hoher Linearität und Messgenauigkeit erreicht. Verbesserungen im Bereich der lateralen Quantifizierung von Bor sind dringend notwendig, da die lokale Auflösung durch die Inhomogenität der Proben limitiert ist. Deshalb sind Verbesserungen in der Probenherstellung und damit einer Erhöhung der Analyt Homogenität anzustreben und das Anschaffen von zertifiziertem Standardmaterial in Betracht zu ziehen. Zuletzt, sollten mehrere Exemplare der untersuchten Proben hergestellt und gemessen werden um die Resultate validieren und statistisch absichern zu können.

Acknowledgement

The last six years of my academic career have enriched my life in so many ways. With its high quality education and exemplary support, the University of Technology in Vienna prepared me for future tasks. Also, I am very thankful for the opportunity to have been part of an unforgettable experience as an exchange student at the North Carolina State University.

First, I want to thank my supervisor Andreas Limbeck for the offer to work in his group, his valuable support and dedicated input, which he contributed with to my master's thesis. Then, I want to thank the working group for making this experience such a wonderful and fun one.

My thanks also go to Christian Gierl-Mayer, my co-supervisor, for his contributions to troubleshooting with his profound expertise. Moreover, I want to express my appreciation to both supervisors for promoting collaboration between their working groups and allowing me to be part of it.

Next, I want to thank Max Bonta for having the patience and endurance to help me overcome many obstacles connected to my project and always assisting me with valuable input. Furthermore my thanks go to Matthias and Dodo, my first and best friends with whom I went through thick and thin. Elke, for always lightening up my mood and keeping me motivated. Alex, Valentin, Christoph, Robert, Elise, Georg, Lukas and all the others who accompanied my life on and off university and I consider great friends.

My love Sanja, my greatest fan and critic, who always stands by my side no matter what.

Finally I want to thank the greatest people on earth, my parents Jan and Monika and my sister Katarina. Thank you for always believing in me, supporting and loving me.

Table of Content

Introduction

The activating effect of boron on the sintering of iron was already published in 1955[1], and described by many authors over the years[2]. But still there is no real industrial application for different reasons. One of the major problems is the reactivity of the added boron with usual sintering atmospheres.

The sensitivity for the formation of brittle phases with boron at grain boundaries is system immanent, because one of the most important precautions for activated sintering is the low solubility of the liquid phase in the matrix to assured during the whole sintering process. If this phase is a brittle, as it is with boron addition, mechanical properties (especially the elongation of the material) are strongly dependent on the presence or absence of a continuous network. Some alloying elements such as chromium influence the solubility of boron however, there still exists a limit of boron addition to avoid embrittlement of the material. It is interesting to know how much boron can be dissolved within the matrix, but boron as a light element is very tricky to analyse quantitatively. All physical methods based on X-rays are not very sensitive due to the low atomic number of boron.

The new method of LA-ICP-MS laser-ablation Inductively Coupled Plasma Mass Spectrometry (Laser-Ablation Inductively Coupled Plasma Mass Spectrometry) provides the possibility to analyse boron quantitatively in a lateral manner. The method is based on the evaporation of the sample with a focused laser beam the transfer of the evaporated material into Ar-plasma and the subsequent element specific analysis of ions with a mass spectrometer. LA-ICP-MS is a highly accepted, widely used method for the determination of major, minor and trace elements in solids as well as isotope-ratio measurements[3]. Spotwise ablation of sample material enables lateral analysis. Major limitations associated with LA-ICP-MS are the non-sample related variation of the analytic response during the ablation process, defined as elemental fractionation[4].

---

[1] (Benesovsky, Hotop, & W.Frehn, 1955)
[2] (Madan, German, & James, 1986)
[3] (Günther & Hattendorf, 2005)
[4] (Mokgalaka & Gordea-Torresdey, 2006)

The emphasis of this work was to develop a method which enables quantification of boron in PM-samples via LA-ICP-MS. Also physical and metallographic examination was performed in order to support results and statements provided by analytical measurements of boron.

Abbreviations

EDS	Energy-Dispersive X-Ray Spectroscopy
ICP-MS	Inductively Coupled Plasma Mass Spectrometry
ICP-OES	Inductively Coupled Plasma Optical Emission Spectrometry
LA	Laser Ablation
LOD	Limit of Detection
m/z	mass-to-charge ratio
PM	Powder Metallurgy
Q-MS	Quadrupole Mass Spectrometry
RSD	Relative Standard Deviation
SEM	Scanning Electron Microscopy

1. Theory

1.1. Boron in powder metallurgy-steel

The application of boron in powder metallurgy (PM)-steels has been confirmed to be an excellent method to enhance the sintered density of the final piece. In general, boron can be applied as an elemental powder or as a so called masteralloy to the steel before being atomized. In either case said element forms a "low melting eutectic" that allows liquid phase sintering.[5]

In materials which were obtained by techniques applied in powder metallurgy, boron is added as a sintering activator in order to form that liquid phase. Concerning ferrous materials, boron is known to act as an ideal sintering enhancer.[6,7]

Apart from the elements noted in classic metallurgy such as Ti, Ca, Al, Zr, B and forth, it is the element boron which is the most attractive one.[8] The similarities between carbon and boron concerning their diffusion coefficient allow the latter to be used for activated liquid phase sintering.[9]

Apart from all mentioned advantages which boron offers as a constituent for activated sintering, there are still a lot problems and limitations concerning the usage of this element in that particular aspect which have to be considered.

First, it has been reported that particular sintering gases can interact with boron during sintering. Gierl, Moshin and Danninger suggest that in the presence of nitrogen as a sintering gas h-BN can be formed leading to the "deactivation of the boron source".[10,11] If hydrogen is supplied during the sintering procedure the formation of B_2H_3 is reported. Consequently, a gradual loss of boron from outside to inside is observable resulting in a "gradual deactivation" of the sample. This means that the only logical conclusion is to use vacuum conditions for

---

[5] (Schade, Schaberl, Thakur, & Dongre, 2005)
[6] (German & Rabin, Powder Metall. 28, 1985)
[7] (Madan D. , 1991)
[8] (Houdremont, Special Steels vol 1 and 2 [Russian Translation], 1966)
[9] (Bendereva & Vylkanov, 2012)
[10] (Gierl, Moshin, & Danninger, 2008)
[11] (Vassileva, Danninger, & Gierl, 2007)

sintering, if wanting to prevent the loss of boron due to the formation of volatile compounds. For the processing of "PM structural parts", the latter is known to be uneconomic.[12]

What is more, excessive concentrations of boron tend to form a high quantity of liquid phase during sintering. In the following, segregation of said liquid phase will take place at the grain boundaries forming a continuous network of solid phase which contains high amounts of boron.[13] These Fe_2B and FeB type eutectic, network-like structures exhibit high hardness (1430-1480 HV and 1800-2000 HV, respectively). However, the morphologies of the borides exhibit the continuous interconnected brittle network which destroys the continuity of the matrix and reduces the toughness of the steel.[14] Therefore, the amount of boron employed as the activated sintering agent has to be taken into account when performing sintering processes.
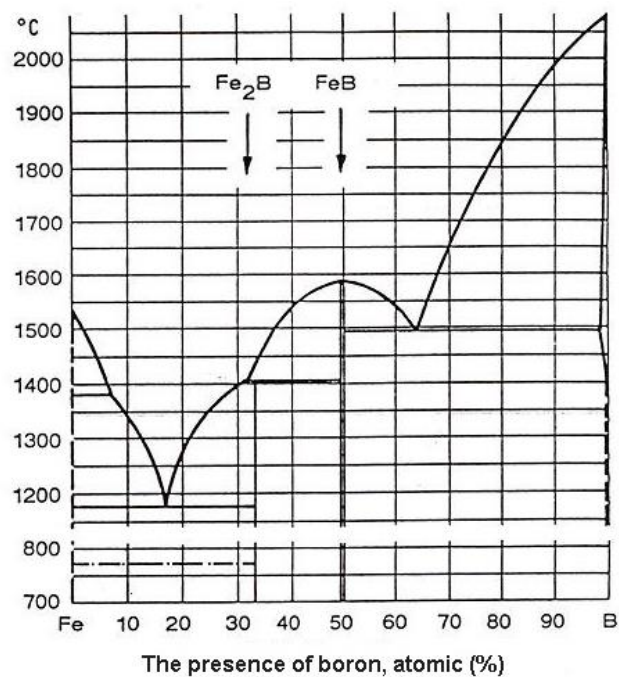

Figure 1 - calculated Fe-B binary phase diagram[15]

Figure 1 presents a binary phase diagram for the compound Fe-B. At about 17 atomic% B and 1174 ∘C, a low melting eutectic, intermetallic compound, namely Fe_2B, is existent which is rich

---

[12] (Selecka & Bures, Metallography 1998, 1998)
[13] (Röttger, Weber, & Theisen, 2012)
[14] (Zhang, Li, Wei, & Zhao, 2011)
[15] (Yoshitomi, Nakama, Ohtani, & Hasebe, 2008)

in iron. Furthermore, boron exhibits a low solubility in iron and whereas for the solubility of iron in boron the contrary is observable. That behavior forces the segregation of a layer on particle surfaces and along grain boundaries which contains large amounts of boron. This process takes place at the very beginning of the sintering. Generally speaking, raising the amount of boron which is added to the material leads to a larger quantity of the eutectic phase which will ultimately cause densification of the material, rounded pores and enhanced mechanical properties. At optimized sintering conditions (temperature and boron content) almost complete dense parts are achievable.[16]

"Within the range between these two eutectics, the liquidus temperature varies between 1149°C, the eutectic temperature at 17 atomic percent of boron, and 1590°C for the alloy with 50 atomic percent of boron. Accordingly, the melting temperature of iron can be lowered by more than 150°C to the maximum of 350°C (at 17 atomic percent of boron) by addition of 5 to 30 atomic percent of bor. By increasing proportion of boron in the ferroboron from the second eutectic, the liquidus temperature rises steadily and almost linearly up to the melting temperature of pure boron. Accordingly, in the above diagram, iron boride (FeB) has 16.23 weight percent of boron, a rhombic lattice and extreme hardness of 2300 HV0.2. Iron-II-boride (Fe_2B) has 8.83 weight percent of boron, a tetragonal lattice and hardness of 1800 to 2000 HV0.2 (preferable as long as FeB is being avoided).

Many authors have made more precise investigations of the iron/boron binary system in the iron rich corner.
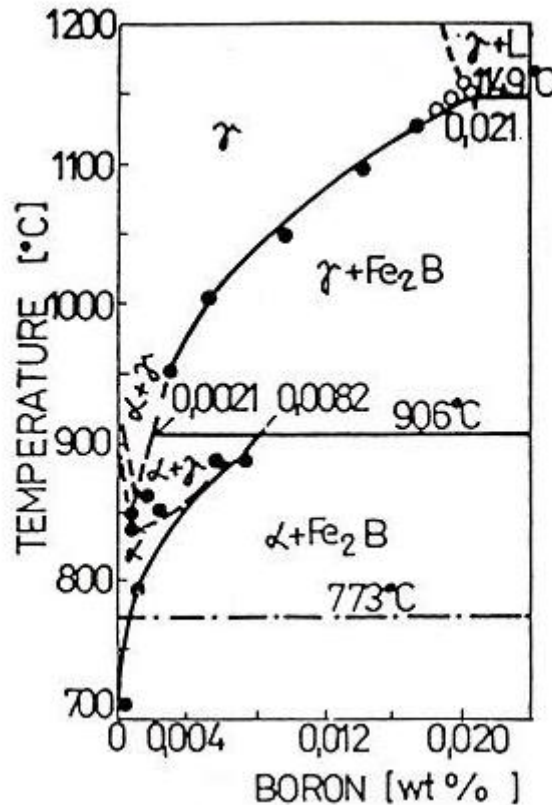
---

[16] (Selecka, Salak, & Danninger, 2003)

Figure 2 - binary FeB phase diagram for low boron concentrations[17]

According to Houndremont's binary phase diagram Fe-B, which is shown in Figure 2, in the low concentration region of boron the maximum solubility of boron is 0,021% at 1149°C. At the same time, with the temperature decrease its solubility decreases too, namely down to 0.0021% at 906°C.

Simultaneously this temperature is perytectoide for perytectoide reaction at 0.0082%B. Boron solubility in γ-Fe suddenly decreases and at 710°C only about 0.0004% of boron substitionally dissolved."[18]

1.2. Activated sintering

Activated sintering lowers the "thermal activation energy barrier" of the sintering process. This results in decreased sintering temperature as well as sintering times. Also, it leads to improved material properties. In order to provide enhanced diffusion during sintering a proper agent for activated sintering needs to be defined. This decision-making is generally based on the phase diagram features.[19]

---

[17] (Houdremont, 1956)
[18] (Key to Metals AG, 2007)
[19] (German, Int. J. Powder Metall. & Powder Technol., vol. 19, no. 4 , 1983)

Liquid Phase Sintering and activated sintering are two techniques which are designed to support the sintering process.

The most important characteristic of Liquid Sintering, is that the sintering temperature is set above the melting point of the sintering additive so that a molten binder phase is formed and preserved during sintering. For said liquid phase, substantial amounts up to quantities of "40 percent by weight" are achievable.

Activated sintering is performed in the presence of small quantities of metal additives. In contrary to the technique of liquid phase sintering, it occurs in the solid state which means that sintering temperature is set below the melting point of the additive. Therefore, activated sintering can be performed at lower temperatures compared to sintering in the liquid phase, however not necessarily since it is dependent on the distinct metal additive applied. Nevertheless, it can be definitely claimed that for both liquid- and activated sintering, temperatures are substantially lower than otherwise required if sintering would be performed without the application of additives.[20]

When comparing activated sintering to single phase, solid state sintering, similarities in terms of their predominant mechanisms for material transport can be defined. In activated sintering, the most dominant process is the diffusion of the base metal through grain boundaries which are rich in additives. Additionally, surface diffusion on free surfaces can be examined. The schematic model for the transport process, provided by the additive is displayed in Figure 4. The activator layer which is formed in between the particles provides a short cut for the mass transport so that it can form the sinter bond more rapidly. In that regard, the sintering activator functions as an enhancer for diffusive transport by lowering the process activation energy (E_A). However, it has to be pointed out that activated sintering only occurs if the additive stays segregated as a grain boundary phase. That segregated phase to work as a sintering activator as efficiently as possible, following conditions have to be preserved: First, the additive needs to form a "low melting temperature phase". Second, as the concentration of additive increases, the liquidus and solidus temperatures are required to decline in order to promote segregation. Moreover, "wetting of the grain boundaries" and the "continuity of this layer" are prerequisites for high efficiency in activated sintering. It is considered that mild

---

[20] (Corti, 1986)

solubility of the base metal in the sintering additive optimizes the process as well. A sketch of a model binary phase diagram covering all mentioned features is presented in Figure 3.[21]
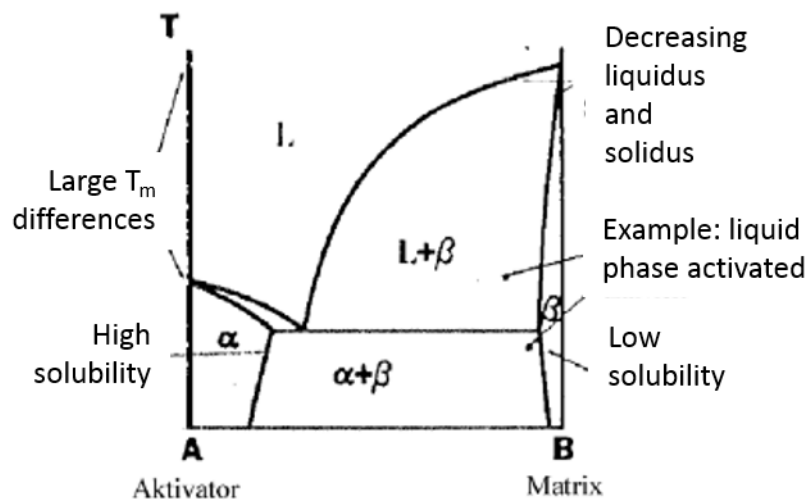

Figure 3 - ideal binary phase diagram for activated sintering[21]

The characteristic phase reactions as shown in Figure 3 proceed in many systems exhibiting activated sintering.[22]

Generally speaking, activated sintering is defined as any special process targeted at enhancing the sintering rate.[23] There are several factors which have to be kept in mind when dealing with activated sintering processes. In simplified terms, the rate of sintering is viewed as dependent on certain parameters which are taken into account in Equation 1 , a model for pore elimination.

Equation 1 - sintering rate[21]

$$\frac{d\epsilon}{dt} = -\frac{g \cdot \exp(-E_A/RT)}{\epsilon^{1,2} \cdot G^3} \cdot \left[\frac{\gamma}{r} + P\right]$$

ε… porosity
t… time
g… a collection of geometric and material constants
Q… activation energy
R… gas constant
T… absolute temperature
G… grain size
r… pore size
γ… surface energy
P… effective pressure

---

[21] (German, Int. J. Powder Metall. & Powder Technol., vol. 19, no. 4 , 1983)
[22] (Zovas & German, 1983)
[23] (German & Munir, Reviews Powder Met. Phys. Ceram., 1982)

In solid state sintering, the grain size G as well as the activation energy E_A are predominant factors. According to the model for pore elimination, a small activation energy and small grain size both enhance densification obtained with sintering. E_A has the greatest effect on the sintering rate $d\varepsilon/dt$ which can be seen in Equation 1.

The main objective in activated sintering is to improve the sintering process by facilitating diffusion, usually by "providing a short circuit diffusion path", and decreasing its activation energy. Considering the latter, sintering time and temperature can be reduced. Also, improved sample properties can be obtained.[24]

The effect of additive concentration on densification in activated sintering has been investigated in various work.[25] The minimum amount of particular activator is limited to approximately one atomic monolayer on the base metal particle surface. Additive contents above the optimum don't improve activated sintering anymore, quite the contrary, sintering efficiency is decreased. Furthermore, the process is also very "sensitive to the uniformity of activator distribution".[26]
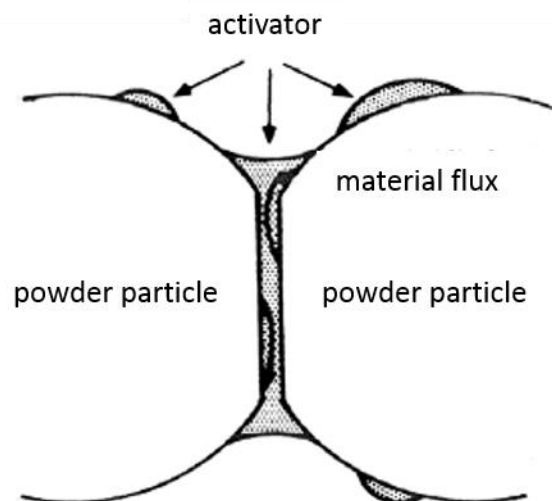
Figure 4 - geometric model for diffusional activated sintering[27]

[24] (German, Int. J. Powder Metall. & Powder Technol., vol. 19, no. 4 , 1983)
[25] (German & Munir, Reviews Powder Met. Phys. Ceram., 1982)
[26] (German, Int. J. Powder Metall. & Powder Technol., vol. 19, no. 4 , 1983)
[27] (German, Int. J. Powder Metall. & Powder Technol., vol. 19, no. 4 , 1983)

1.3. Measurement of boron with ICP-MS

The inductively coupled plasma mass spectrometry (ICP-MS) applies the principle of analyte ionization in an Ar-plasma and is the most widely used plasma based technique for the analysis of boron. The advantages of the ICP-MS over other methods are higher sensitivity, lower detection limits, and simultaneous measurement of ^{10}B to ^{11}B isotopic ratio.[28] The reported detection limits are at the ppb level, depending mostly on the sample type.[29]

The element boron has two stable isotopes, ^{10}B and ^{11}B, respectively. Boron isotope ratio data are usually reported relative to NIST-SRM951. Relevant data is presented in Table 1.

Table 1 - stable isotopes of boron, isotopic mass and abundance[30]

boron isotopes	Isotopic mass [u]	abundance [%]
^{10}B	10.013	19,9
^{11}B	11.009	80,1

When comparing to other measuring techniques, an important benefit of the ICP-MS becomes apparent. In techniques which are based on the principle of measuring light absorbance, several spectral interferences occur with a number of elements because the wavelength of boron is close to the wavelength of these elements. Eaton and Franson report "interferences with Fe, Al, Ni, Cr, Si and V for ICP-OES."[31]

One of the positive aspects of the quantification of boron with ICP-MS is that there aren't any noticeable elemental interferences that need to be considered. Also Boron determination is unaffected by isobaric or spectroscopic interferences.

Another aspect that has to be considered is mass fractionation. It occurs due to "space-charge effects", which result in unequal and preferential transmission of the heavier isotope through the machine parts. When the heavier isotopes pass through the components of the ICP-MS they are delayed compared to the lighter isotopes. Consequently, detected signal intensity of the heavier isotope will decrease which means that the reported concentration will be lower. This will cause a substantial alteration in the isotope ratio. Regarding the ICP-MS analysis of boron, mass fractionation is inevitable when monitoring low masses such as 10 and 11 for ^{10}B

---

[28] (Brown & Hu, 1996)
[29] (Sah & Brown, 1997)
[30] (IUPAC, 1998)
[31] (Eaton & Franson, 2005)

and [11]B, respectively. However, the measurement of the total boron concentration in the sample is not significantly affected by these circumstances.[32]

1.4.   Laser Ablation (LA)

Laser ablation is a method which can be used for multielement analysis in solid samples. Also, basically no sample preparation processes are needed to be performed in order to conduct measurements. Analyzing the sample without having to care about sample preparation processes provides several benefits, such as minimization of contamination, elimination of dilution errors and loss of volatile elements.

For LA the sample is positioned in a so called ablation chamber which is airtight and purged with a carrier gas such as helium or argon. Next, the laser beam is focused and applied on the sample. Particles are ablated from the sample surface via thermal heating generating an aerosol of a certain particle size distribution. The vapor and particulate matter is carried by the particular carrier gas through an ablation cup into the plasma where the ionization process takes place. The instrumental set-up of a laser ablation system is illustrated in Figure 5. The spot diameter of the laser beam can be varied, leading to a spatial resolution between some μm and several hundred μm (has a great impact on the signal intensity of investigated analytes). These circumstances enable a quasi-nondestructive analysis of samples when using smaller laser diameters.
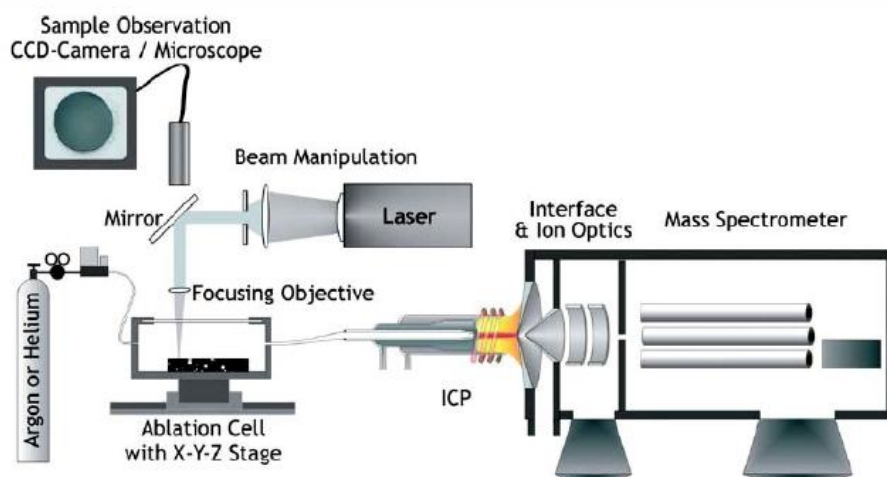
Figure 5 - schematic set-up of a Laser Ablation system, coupled with a ICP-MS[33]

---

[32] (Rao, Parab, Sasibhushan, & Aggarwal, 2009)
[33] (Günther & Hattendorf, 2005)

The Laser-wavelength, the kind of carrier gas used and its flow rate, pulse duration of the laser as well as the pulse energy and finally the particle size are some of the major parameters which have an influence on the vaporization and ionization processes of the sample material. Wavelengths of most lasers are located in the UV-range (266, 213 and 193 nm) whereas shorter wavelengths minimize thermal alteration of the sample material. The latter can be achieved as well by reducing laser pulse duration for example by using a fs-laser. In general, ns-laser are the most commonly used laser types in LA systems. A more widespread use of fs-lasers is currently limited by their high acquisition costs. Investigations on metallic suggest that the pulse duration of the laser has more of an impact on the ablation characteristics than its wavelength has. It has also been observed that improvements in signal can be obtained by using helium as a carrier gas. Moreover, since the signal intensity is directly proportional to the quantity of ablated material carried into the ICP, adjustments in laser spot diameters have to be taken into consideration. That being said, increasing the laser diameter will ultimately lead to better detection limits for particular analytes.

In general, the analysis task has to be considered when deciding upon the size of the laser diameter. When performing investigations on the distribution of particular analytes, a small laser diameter should be chosen for measurements in order to improve resolution. Whereas when investigating in bulk characteristics, larger laser diameters are preferred. Moreover, it is important to provide sufficient amounts of ablated and analyzed sample material in order to assure representative results even for samples which exhibit inhomogenously distributed constituents.

Yet, LA-ICP-MS measurement of solid samples requires matrix matched calibration standards, since the ablation process is strongly matrix dependent, which is also the downside of that instrumental analysis. These so-called matrix effects are based on different absorption of the laser which leads to variations in sample input into the plasma.[34]

Furthermore, major limitations associated with LA-ICP-MS are the non-sample related variations of the analyte response during the ablation process, defined as elemental fractionation. More precisely, the ablation of the material produces a stream of particles with a heterogeneous size distribution which is transported as an aerosol into the ICP and can cause elemental fractionation. Large particles can lead to an incomplete evaporation process within

---

[34] (Mokgalaka & Gordea-Torresdey, 2006)

the plasma resulting in an aberration of isotope ratios and ultimately in poor analytical precision and accuracy. Also, thermal effects occur when analyzing solid samples via LA (Figure 6).

In general, elemental fractionation is dependent on the laser wavelength. The shorter the laser wavelength, the higher the ablation rate and the lower the fractionation. Hence minimization of the said effect can be achieved by decreasing the laser pulse duration down to the femtosecond (fs) range as well as the wavelength of the laser.

The amount of material transported from the ablation site to the plasma source for ionization can be a limiting factor towards the sensitivity of the ICP-MS instrumentation used. That being said, carrier gas flow is an important factor which has to be adjusted to optimal conditions in order to prevent particle loss during transport.[35]

Because of all the reasons mentioned above, reference material with similar matrices to the samples need to be measured to generate a calibration function. However, reference materials are not commercially available for all the different matrices. In many cases, reference materials have to be manufactured in-house.
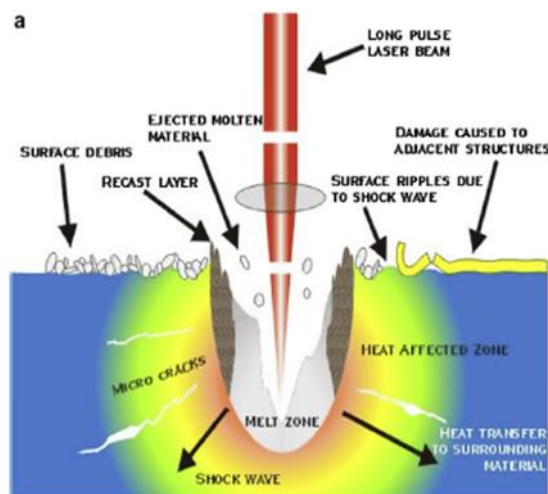
Figure 6 - complex processes during sample ablation via laser[36]

---

[35] (Mokgalaka & Gordea-Torresdey, 2006)
[36] (Fernandez, 2007)

1.5. Inductively Coupled Plasma (ICP)

Inductively coupled plasma (ICP) is commonly used in analytical atomic spectroscopy. The principle of ICP is based on the transformation of either a gaseous, liquid or solid sample into an aerosol and its subsequent transportation into the plasma. The analytes are introduced either as a wet or a dry aerosol, deriving from liquid and solid samples, respectively. The aerosol is carried into the plasma via a carrier gas through the inner tube of the plasma torch and transported into the argon plasma. In the plasma the vaporization-atomization-excitation-ionization process takes place. This process is dependent of the plasma temperature.[37]

 The plasma is formed in a stream of argon-gas which flows through the plasma torch, consisting of three concentric quartz tubes. The design of said plasma torch is contributed to the adherence of constant, homogenous gas flow, resulting in stable plasma conditions. Hence constant temperature in the plasma can be obtained leading to reproducible analysis.[38] The plasma torch is enwrapped by an induction coil which is connected to a radiofrequency (RF) generator and cooled with argon gas. The inside of the quartz tube is cooled down by a second stream of cooling gas which is mostly done with a stream of argon that provides a vortex flow. Such composition of a plasma torch can be seen in Figure 7.

As long as a continuous argon gas flow is present and the magnetic field strength properly adjusted, stable plasma conditions are assured. When molecules enter the plasma, they are vaporized, atomized, excited and ionized, in that particular order. Depending on the device, emitted radiation (ICP-OES) or ions (ICP-MS) can be detected. Plasma temperature usually varies between 6000 - 10000 K depending on the RF energy and applied gas flow. Also, a high electron number density ($1-3 \times 10^{15}$ cm^{-3}) is one the main characteristics of an argon ICP. The Residence time of the sample aerosol in the plasma is about 2 - 3 ms. The vaporization to atomization process takes place in an almost chemically inert environment. Because of these characteristics which are typical parameters for the use of an argon ICP, this instrument is commonly used for simultaneous multielement analysis. Moreover, argon ICP enables the detection of a wide variety of elements from main constituents down to trace- and ultratrace concentration levels. Additionally, this method provides the advantage of low-noise

---

[37] (Koch & Günther, 2011)
[38] (Nischkauer, 2011)

conditions. Figure 7 shows the possible variations of the temperature depending on the location in the plasma torch.
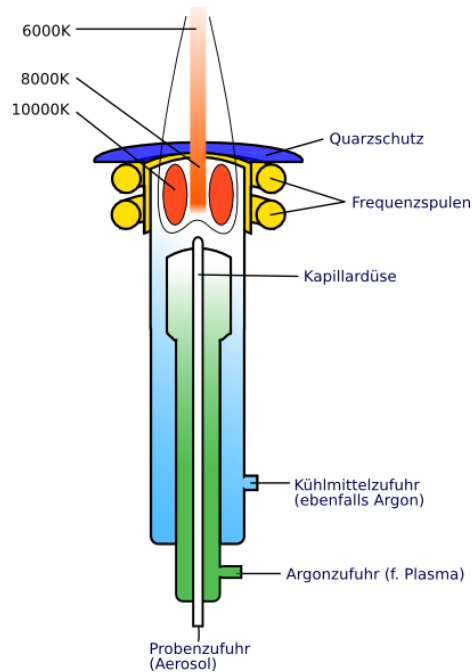

Figure 7 - temperature zones in an ICP-torch[39]

Due to the high plasma temperature and the long dwell time of the sample aerosol in the plasma, the excitation-ionization process of said aerosol is conducted almost completely. What is more, the chemical and physical interferences are reduced.

1.6.   Inductively Coupled Plasma Mass Spectrometry (ICP-MS)

Over the last years, inductively coupled plasma mass spectrometry (ICP-MS) has become an important analysis method for inorganic trace- as well as ultra-trace analysis. Some of the instruments benefits are its low detection limits, down to ppt-scale (pg/L) and the possibility of simultaneous multielement analysis. Also the ICP-MS brings high sensitivity and broad dynamic range to the table. Another upside is the option of isotope analysis.[40]

---

[39] (wikipedia.org, 2004)
[40] (Günther & Hattendorf, 2005)

1.6.1. Sample Introduction

In case of LA-ICP-MS, sample introduction is crucial for the production of ions and interfering species. The interaction of laser beam and sample material produces thermal heat which results in the production of an aerosol. The latter is then transported into the plasma with a carrier gas.

With liquid sample introduction, the sample is converted into an aerosol via a nebulizer. The aerosol then passes through a peltier-cooled spray chamber in which large aerosol droplets are separated from the small ones, hence only the latter are transported into the plasma. By doing so, effective ionization of the ablated sample material is assured. In this work, a concentric pneumatic nebulizer and a cyclonic spray chamber were used. Furthermore, the set-up of a calibration function for quantification is simplified by the use of aqueous standard solution, which is a great benefit.

As mentioned before, analytes can be introduced to the plasma via gas phase. The analytes are transferred into a gas phase and then introduced into the ICP, for example through coupling with a gas chromatograph (GC) or supercritical fluid chromatography (SFC).[41]

1.6.2. Sample Ionization

In the plasma, which is described in 1.5, dissociation of molecules and ionization of atoms takes place. The plasma contains a temperature gradient which is presented in Figure 7. Ions are formed in hotter areas of the plasma. However, merging or the formation of polyatomic species can occur in colder areas of the plasma. Detection of these polyatomic ions can lead to spectral interferences. More precisely, polyatomic species often have similar masses as other single atomic ions and are therefore detected on the same mass. However, spectral interferences can be disabled. In order to prevent falsified results, it is advisable to measure more than one isotope of the analyte. By doing so, one can check the isotope ratio, which has a defined numerical value (since each isotope has a specific abundance) for discrepancies and tell if the measured ions are only analytes or if spectral interferences are present.[42]

---

[41] (Koch & Günther, 2011)
[42] (Thomas, 2001)

1.6.3. Interface

Inductively coupled plasmas are operated under atmospheric pressure, whereas the detection of ions in an ICP-MS is performed under high vacuum. The high vacuum is necessary in order to decrease the amount of gas molecules, resulting in less collisions with analyte ions and leading to an increased transmission of them. Therefore, vacuum needs to be at least 10^{-5} mbar (typically it varies from 10^{-7} to 10^{-8} mbar). The MS interface provides an intermediate region which connects the regions of atmospheric pressure and high vacuum.

The structure of an ICP-MS interface is illustrated in Figure 8. It is built up by two stages which are called the sampler- and skimmer-cone. Those metallic parts usually consist of nickel. What is more, platinum cones can be used for special applications. The so called sampler cone is facing the plasma torch and separating the atmospheric pressure from the intermediate vacuum zone. The latter is governed by a pressure of about 1 mbar. The skimmer cone which is placed behind the sampler cone, transits from intermediate vacuum to high vacuum. The diameter of the hole of the skimmer cone is approximately 1 mm and should be as large as possible in order to maximize the analyte signal and minimize orifice clogging while keeping the extraction pumps small.[43]
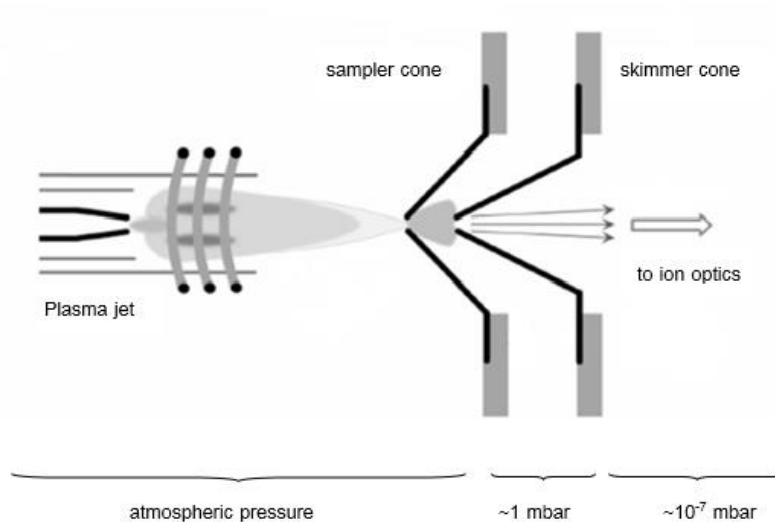
Figure 8 - illustration of a typical ICP-MS vacuum interface[44]

---

[43] (Koch & Günther, 2011)
[44] (Bonta, 2013)

1.6.4. Ion Focusing System

The Ion Focusing System is located after the skimmer cone and it has the important task to focus the ion beam before it enters the mass analyzer. The ions enter into the vacuum unfocused after being extracted from the plasma to the high vacuum area. Consequently this will lead to beam expansion. Hence, an ion optic system is installed which refocuses the ions again in order to form a sharp beam.

This optical system is comprised of one or more ion lenses, which guide the analytes electrostatically from the interface directly into the MS. The goal of the ion focusing system is to transport the maximum number of analyte ions into the MS. Simultaneously, it rejects as many of the matrix- and non-analyte-based (e.g. photons) components as possible. Also, it is stopping particles, neutral species and photons from entering into the mass spectrometer device since these components lead to high background noise when reaching the detector. In order to prevent the latter a metallic disc ("photon stop") is placed at the center of the lens system. This photon stop prohibits a direct line of sight between the detector and the plasma and prevents plasma produced photons from reaching the detector. Low background counts, better detection limits and stable signals are enabled because of the ion focusing system. An additional instrument placed in inside the ion focusing system in order to stop unwanted species from reaching the detector is the application of a 90° deflection lens. Analyte ions are deflected towards the detector, which is arranged at an angle of 90° from the primary ion beam. Photons and other unwanted species are not deflected, thus they never reach the detector.[45]

1.6.5. Mass Analyzer

In short, the mass analyzer separates the ions according to their mass-to-charge ratio. More precisely, the main objective is to divide the analytes from the ions that are of no interest such as matrix, solvent and so forth. Mass separation devices are operating between the ion focusing system and the detector. There are three different types of mass analyzers available at the moment which are differing from each other in their principle of mass separation. Those are the sector field MS, the time-of-flight (TOF) MS and the quadrupole MS. The latter is by far

---

[45] (Thomas, 2001)

the most common mass separation device. What is more, the quadrupole MS was utilized in this work, thus this device will be discussed more precisely.

The sector field MS uses a static electric or magnetic sector or some combination of the two for mass-separation and is commonly used in combination with LA-ICP-MS as well. On the contrary, TOF-MS were only commercially available for a short period.

Q-MS are widely used because of their relative simplicity, good performance, high-throughput and low cost. As illustrated in Figure 9, a quadrupole is built-up of four cylindrical metal rods, made of stainless steel or molybdenum and sometimes with a ceramic coating for corrosion resistance. Their dimensions are about 1 cm in diameter and 15 to 20 cm in length.
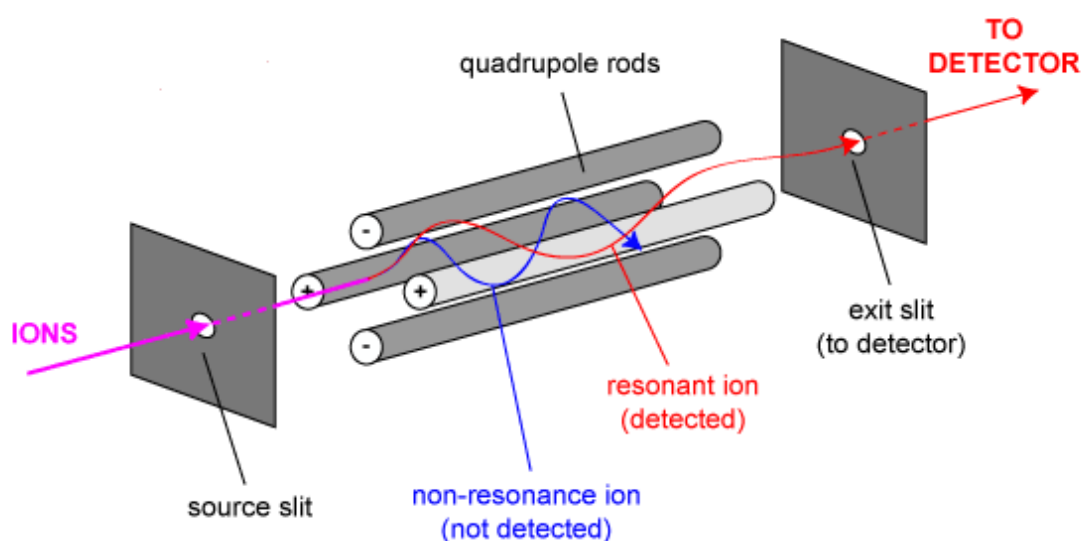
Figure 9 - Quadrupole Mass Separation Device[46]

When ions enter the quadrupole a direct current field is applied on one pair and a radio frequency field on the other pair of rods. Consequently, only ions of one selected mass-to-charge ratio are allowed to pass through the quadrupole. Ions of different m/z ratios are deflected by the magnetic field and finally they are either discharged by hitting a rod or they pass through the spaces between the rods. Therefore, those ions will not be detected.

The desired species of ions, hence the analyte, will be electrostatically directed by a negative or positive bias which is generated as soon as a particular voltage is applied to the rods. The detector registers an electrical pulse which is representative of the analyte ion. This sequence is repeated for every m/z desired to be analyzed.[47]

---

[46] (www.slideshare.net, 2014)
[47] (Thomas, 2001)

Yet quadrupoles have their limitations, being sequential instruments and having a relatively low resolution. This low resolution derives from peaks that cannot be separated. High mass resolutions are achievable when using a sector field MS. If there is need for simultaneous detection of the whole mass spectrum, the application of a time-of-flight mass separation devices should be considered.

1.6.6. Detector

Finally, the ions arrive at the detector where they are converted into electrical pulses and counted. The amount of ions hitting the detector is proportional to the magnitude of those counted electrical pulses thus quantification of the analyte is enabled.

Electron multipliers are often utilized as a detector in LA-ICP-MS. In an electron multiplier, the ion enters the detector and impacts on either a semiconductor material (channel electron multiplier) or discrete dynodes (discrete dynode electron multiplier) which generates electrons. These electrons start a chain reaction, generating a multitude of electrons, hence causing a multiplication of the signal.[48]

---

[48] (Thomas, 2001)

2. Experimental

This chapter gives an overview of the instruments and chemicals being used for this work, as well as a description of its sample preparation and characterization is described.

2.1. Sample Preparation

2.1.1. Powder Constituents

For the sample preparation three different powders have been utilized.

- Höganäs Astaloy CrM (96.2 wt% Fe; 3 wt% Cr; 0.8 wt% Mo)[49]

- Kropfmühl UF4 Graphite powder (99.5%, d50 = 5.5 - 7µm)[50]

- Boron (crystalline)

In order to investigate on the distribution of boron in the sample matrix, boron concentration has been increased from 0 to 0.6 wt% and mixed with other constituents as shown in Table 2.

Table 2 - composition of powder constituents in wt% with increasing boron concentration; 1 batch

Sample	Fe [wt%]	C [wt%]	Cr [wt%]	Mo [wt%]	B [wt%]	B [ppm]
Blank	95.719	0.5	2985	0.796	0	0
750	95.647	0.5	2.983	0.795	0.075	750
1500	95.575	0.5	2.981	0.795	0.15	1500
3000	95.430	0.5	2.976	0.794	0.3	3000
6000	95.142	0.5	2.967	0.791	0.6	6000

Boron concentration is also given in ppm since it is a common way of quantification in analytical chemistry. Therefore, sample names refer to boron concentration in a particular powder mixture.

---

[49] (Höganäs AB, 2013)
[50] (Graphit Kropfmuehl/AMG Mining AG, 2013)

Three batches of these powder mixtures were processed in total for further investigations (Table 3).

Table 3 - description of sample batches, different atmospheres and utilization

Batch ID (e.g. 750-…)	Sintering atmosphere	Application
-Ar	Argon	Investigated samples
-H2	Hydrogen	Investigated samples
-vac	Vacuum	Method calibration

2.1.2. Mixing of Powder Batches

Argon and hydrogen sintered batches were mixed in a tubular mixer. However, vacuum sintered samples were blended in a tumbler with cyclohexane for about 2.5 hours. A serial dilution was established for enhancing homogeneity of the powder mixture. The following procedure has been applied to each fraction displayed in Table 4.

Table 4 - serial dilution for mixing of vac-batch; starting with Mix A samples of different boron concentration as shown in Table 2 have been achieved consequently

Name of fraction	Concentration of boron [wt%]	Dilution factor
Mix A	10	1:10
Mix B	1	1:10 of Mix A
Vac-Standards (e.g. 750-vac)	Sample series as in Table 2	dilution of Mix B

Also a grinding medium (10 balls of stainless steel) was added for improving mixing efficiency. Since crystalline boron tended to agglomerate on top of the powder pile, ultrasonic disperse was applied to ensure optimum homogeneity of powder components. Solvent was extracted in a rotary evaporator at 40°C and 70mbar till the powder was completely dry (Figure 10).
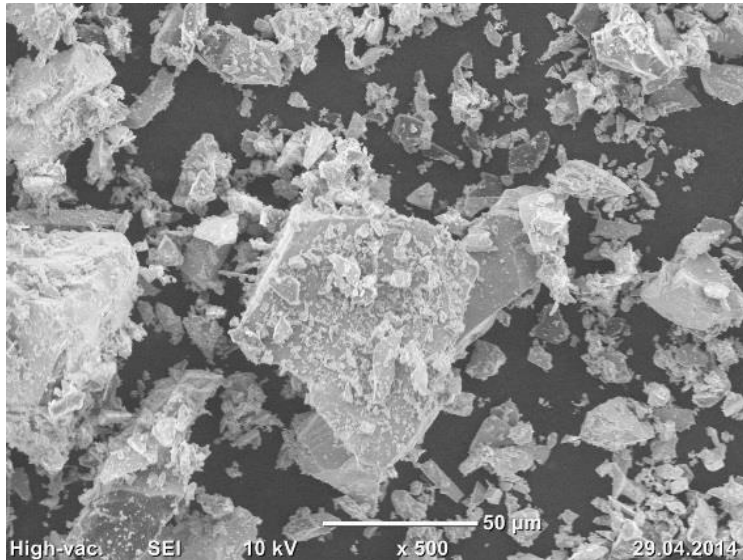
Figure 10 - SEM image of finished powder used for processing vacuum sintered standards (SEI detector, 10kV)

2.1.3. Powder Pressing

For argon and hydrogen sintered batches, samples with the size of 55x10x8 mm³ (Charpy bars) were pressed at 600 MPa in a floating die with die wall lubrication.

0.1g of each powder mixture used for samples sintered in vacuum were grouted with a pneumatic press (pressure of 10 tons for 30 seconds) resulting in a pellet with 13 mm diameter and about 1 mm in height.

2.1.4. Sintering of Samples

Sintering was performed in the dilatometer NETZSCH DIL 402C in argon and in hydrogen (both 99.999 quality) at 1250°C, with a heating and cooling ramp of 10 K/min for 60 min isothermally.

Temperature profile shown in Figure 11 was applied to sintering hydrogen and argon. A different profile was used for sintering in vacuum, where pressure of 0.6mbar could be achieved (and maintained) during the process (Figure 12). For vacuum sintering, dilatometer Bähr Thermoanalyse GmbH type 7125 was used.
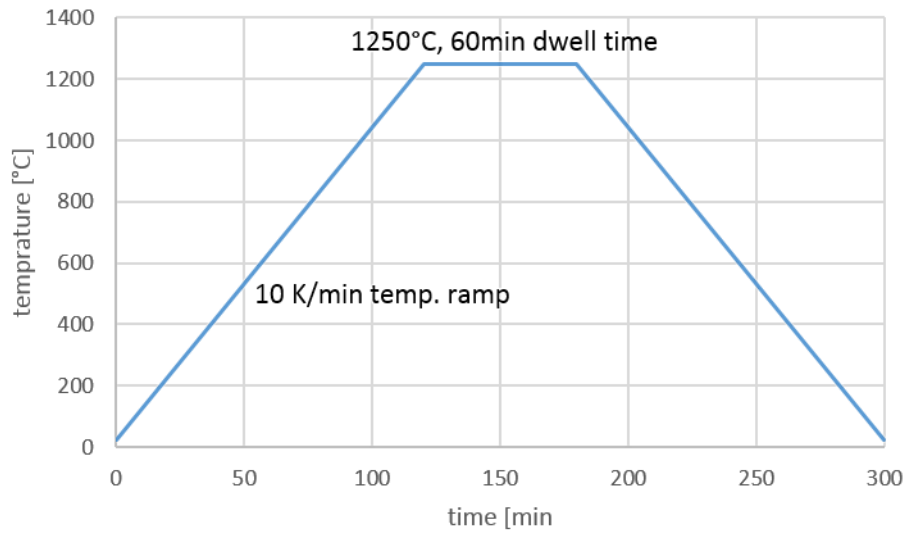
Figure 11 - schematic profile of sintering program applied to argon and hydrogen sintered samples
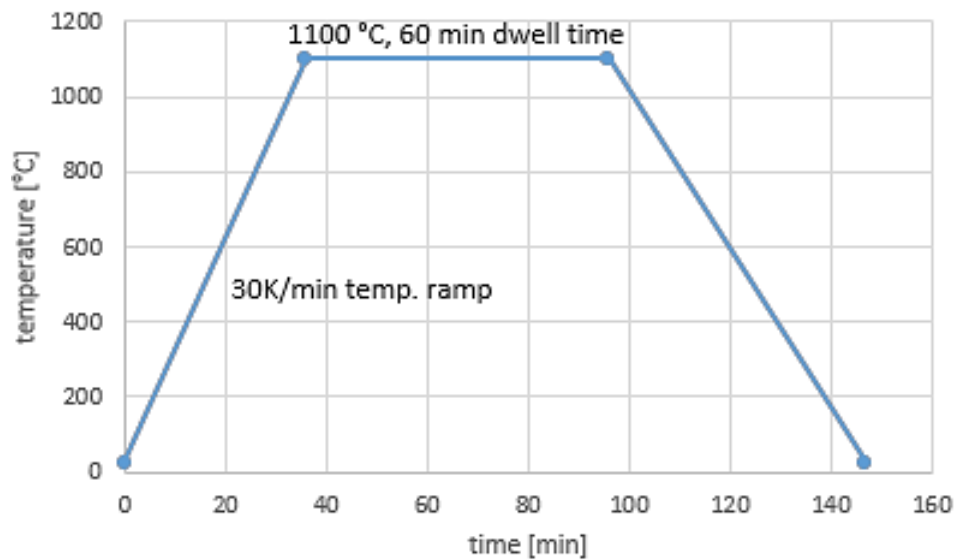
Figure 12 - schematic profile of sintering program applied to vacuum sintered samples

2.2. Sample Characterization

2.2.1. Metallographic Characterization

For surface characterization, fractions of sintered sample cross sections have been mounted in Bakelite for further metallographic preparation. Using STRUERS Tegra Pol-31 with particular grinding and polishing modes, mounted samples have been processed as following (Table 5).

Table 5 - description of modes used for grinding and polishing Ar- and H$_2$-sintered samples; STRUERS Tegra Pol-31

name of mode	plate and lubricant/ grinding medium	duration
Piano	plate: Struers MD piano 220, water	2 min
Allegro	plate: Struers MD allegro, 9 μm diamond paste	7 min
Dac	plate: Struers MD Dac, 3 μm diamond paste	10 min

After each of these steps, samples have been sonicated for 1 minute and cleaned with Isopropanol in order to get rid of eventual contamination. In the next step, samples were polished using Al$_2$O$_3$-Suspension with 1 μm particle size on a 1 μm polishing plate. To finish off the polishing procedure, samples were sonicated and cleaned with Isopropanol again.

Lastly, polished and clean sample cross sections have been etched using a 3% solution of Nital for about 30 seconds and washed off with water and Isopropanol to be ready for metallographic characterization.

2.2.2. Bulk Characterization

To investigate in the densification of argon- and hydrogen sintered samples, density of green bodies and density in sintered state as well as Archimedes density have been examined.

Pre sintered sample bodies have been measured and weighted in order to determine green density using Equation 2. All dimensions (length, width, height and mass) have been determined three times per sample and the average value was used for further calculations.

Equation 2 - Formula for evaluation of green density

$$\rho_{greenbody} = \frac{m}{w \cdot h \cdot l}$$

m… sample mass in green state [g]

w… width of sample body [mm]

h… height [mm]

l… length [mm]

The density of sample bodies in sintered state has been evaluated in two different ways.

First, sample bodies were measured and weighted after being sintered and cooled down to room temperature. The density in sintered state was calculated according to Equation 3. All dimensions (length, width, height and mass) have been determined three times per sample and average value was used for further calculations.

Equation 3 - Formula for evaluation of density in sintered state via geometric dimensions

$$\rho_{sintered\ body} = \frac{m}{w \cdot h \cdot l}$$

m… sample mass in sintered state [g]

w… width of sintered sample body [mm]

h… height [mm]

l… length [mm]

Furthermore, the density of sintered bodies was calculated using Archimedes' principle (Equation 4). Sample bodies were coated with waterproofing spray to hinder water from filling up pores and air dried in a dry box at 90°C for approximately one hour.

Equation 4 - Formula for evaluation of density in sintered state via Archimedes' principle

$$\rho_{Archimedes} = \frac{m_{air}}{m_{air} \cdot m_{H2O}} \cdot \rho_{H2O}$$

m_{air}… sample mass in air [g]

m_{H2O}… sample mass in water [g]

ρ_{H2O}… density of sample in water at 24.2°C [g/cm^3]

2.2.3. Macro- and Micro Hardness

Macro and micro hardness were evaluated on argon and hydrogen sintered samples. Vickers' hardness was the method of choice for investigating macro hardness. In this particular method a pyramid shaped diamond of well-defined dimensions is pressed against the sample with a defined force and causes an impact in the material surface from which a value of Vickers' hardness (HV) can be calculated. Parameters needed for establishing the said value are shown in Equation 5. It has to be mentioned that this method includes the measurement of porosity. For this evaluation, the pre-installed method "HV 30" has been applied. In order to receive

representative and valid average values for macro hardness, five indentations per sample have been made and measured.

$$HV = 0{,}1891 \cdot \frac{F}{d^2}$$

HV… Vickers' hardness [N/m^2]

F… impact force (HV 30 = 294.20 N) [N]

d… average value of diagonals of impact [mm]
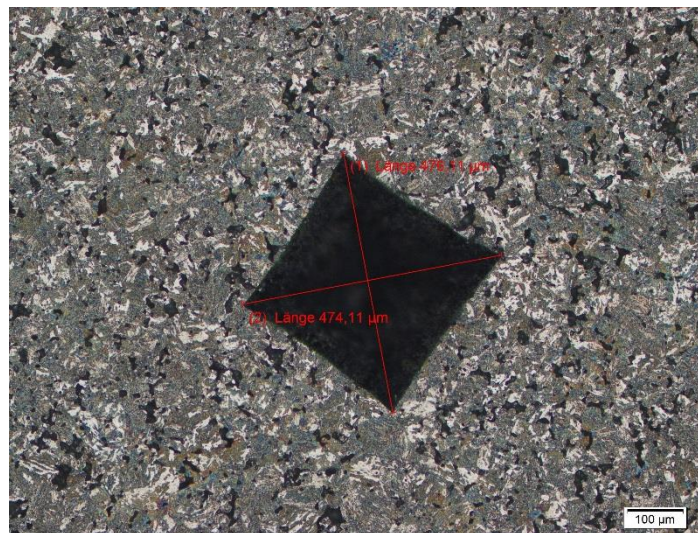
Figure 13 - measured indentation of on sample surface; HV 30

Micro hardness was measured using the micro hardness tester ecoHARD® XM1270A, AHOTEC®. This device makes the characterization of much smaller surface areas possible. That being said, differences in the hardness of boron-rich grain boundaries compared to those of grains have been investigated. Five impacts per characteristic area have been created and then measured and calculated using the devices' software to generate representative values for microhardness.

2.2.4. Impact Toughness

Impact toughness has been evaluated on argon and hydrogen sintered sample bodies (Charpy bars) using a pendulum testing machine. Such a tester is presented schematically in Figure 14.

For both tests, the specimen is broken by a single overload event due to the impact of the pendulum. A stop pointer is used to record how far the pendulum swings back up after fracturing the specimen. The impact toughness of a metal is determined by measuring the energy absorbed in the fracture of the specimen. This is simply obtained by noting the height at which the pendulum is released and the height to which the pendulum swings after it has struck the specimen. The height of the pendulum times the weight of the pendulum produces the potential energy. The difference in potential energy of the pendulum at the start and the end of the test is equal to the absorbed energy.[51]

For both argon and hydrogen sintered batches impact toughness evaluation has been performed on each specimen differing in boron concentration. Equation 6 has been used for calculations.

Equation 6 - Formula for evaluation of impact toughness

$$impact\ toughness = \frac{E}{A}$$

Impact toughness… impact toughness [J/ cm^2]
E… energy of impact (absorbed) [J]
A… area of cross section [cm^2]
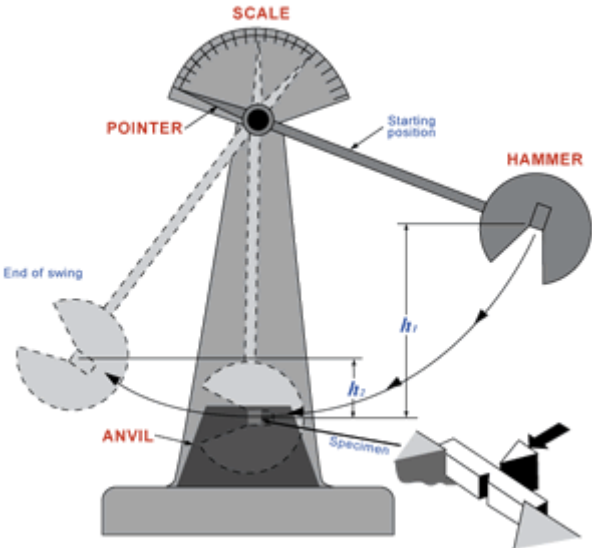
Figure 14 - example of a pendulum-testing machine[52]

---

[51] (NDT resource center, 2015)
[52] (NDT resource center, 2015)

2.2.5. Thermophysical Properties

Dilatometers are high precision systems designed to measure dimensional changes of a specimen brought about by changes in its thermal environment. The linear thermal expansion coefficient, annealing characteristics and other physical or chemical changes manifesting themselves in a change of linear dimension can be precisely determined.

First, for each experiment a fraction of the processed sample green body was loaded into the Dilatometer NETZSCH DIL 402C across direction of measurement. Green bodies where sintered using the temperature/time profile according to Figure 11 in argon and hydrogen atmosphere, respectively. During the said process thermal expansion of samples was measured and plotted against temperature.

2.3. Instrumentation for Chemical Analysis

For the analysis a quadrupole ICP-MS (iCAP Q, ThermoFisher Scientific) was used. For a liquid sample analysis the instrument was equipped with a concentric quartz glass nebulizer and a peltier cooled spray chamber. For a liquid sample introduction the iCAP Q was coupled with an ESI SC-2DXS auto-sampler and a FAST AA sample introduction system (Elemental Scientific, Inc. (ESI)). The software for data acquisition called thermo scientific Qtegra™ version 2.2.1465.24 was provided with the instrument. Such instrumentation is displayed in Figure 15.

Figure 15 - ThermoFisher Scientific iCAP Q; ICP-MS instrumentation for performed experiments

Using a tuning solution (Tune B iCAP Q, Ba, Bi Ce, Co, In, Li, U each 1.0 µg/L in 2% HNO3 + 0.5% HCl, ThermoFisher Scientific) instrument parameters were optimized before each liquid analysis, for maximum ^{115}In- and a ^{140}Ce^{16}O/^{140}Ce signal ratio of ≤ 1.9%.

Table 6 - Parameters applied for iCAP Q, ICP-MS measurements for liquid and solid samples

Parameter	Unit	liquid measurement standard-mode	laser measurements standard-mode
Auxiliary gas flow	L/min	0.80	0.80
Coolant gas flow	L/min	13.0	15.0
Nebulizer gas flow	L/min	0.98	0.80
Dwell time/ isotope	s	0.01	0.01
RF power	W	1550	1550
Cones	-	Ni	Ni
Measured isotopes	-	^{10}B, ^{11}B, ^{115}In	^{10}B, ^{11}B, ^{58}Fe, ^{53}Cr, ^{95}Mo

For the measurement of solid samples the New Wave 213 ESI laser ablation system was utilized and shown in Figure 16. The said instrument was connected to iCAP Q via Teflon tubing of 2mm diameter. A frequency quintupled 213 nm Nd:YAG laser is built in into the New Wave 213. Samples were loaded into a chamber made of an aluminum frame and a plastic bottom where samples had to be attached to via a double faced adhesive tape. This procedure was inevitable since the loaded boron containing metal samples would get magnetized by the laser positioning aperture, attached to it and torn out of the sample chamber. Moreover, samples had to be positioned on the same level vertically to optimize and maintain laser-sample interaction. The ablation cup was kept directly over the ablated spot, to ensure a rapid and constant washout behavior which was performed using Helium as a carrier gas. During all laser measurements dry plasma conditions were applied.

Figure 16 - New Wave 213 ESI laser instrumentation used for performed experiments

Measurement parameters regarding the ICP-MS instrumentation were optimized using a reference material called NIST 612 (National Institute of Standards and Technologies) in order to obtain a maximum ^{115}In signal before every experiment. The applied laser settings for NIST 612 measurements are depicted in Table 7.

Table 7 - standard laser settings applied when measuring NIST 612

Parameter	Unit	Standard settings
Laser beam diameter	μm	80
Repetition rate	Hz	10
Output	%	70
Scan speed	μm/s	5
Carrier gas flow (He)	L/min	0.75
He/Ar-gas flow	L/min	0.75/0.98

2.4. Digestion of Vacuum-Sintered Samples and Preparation of Aqueous Standards

Vacuum sintered samples of different boron concentrations were composed and processed as described in 2.1. Samples were then grinded and fractions placed in PE-tubes for digestion. 1ml of aqua regia (conc. hypochlorite acid and conc. nitric acid; 3:1) was pipetted into the sample containing tube which was then gently heated over night to enhance the digestion process. After that, desired sample solution was pipetted into PE-tubes and diluted to a final volume with 1% HNO_3 (HNO_3 conc. diluted with bi-dest. water). Solution was further diluted using 1% HNO_3 till the preferred concentration of boron was achieved. Solutions of 4 different boron concentrations were manufactured, each represented by 5 specimen.

Standards for ICP-MS analysis were prepared from an ICP-MS calibration standard solution, diluted with 1% HNO_3 (HNO_3 conc. diluted with bi-dest. water). For calibration, a concentration range from 0 ppb to 100ppb boron was evaluated.

ICP-MS measurements required addition of a certain amount of indium (In) stock solution as internal standard. For both digested vacuum-sintered sample solutions and for all aqueous standards a concentration of 1µg/l Indium was adjusted. All chemicals used are shown in Table 8.

Table 8 - Chemicals used for digestion of vacuum-sintered samples and preparation of aqueous standard solutions; ICP-MS measurement

Chemical	Name	Annex	Company
HNO_3	Nitric acid 65%	Emsure® ISO	Merck
HCl	Hypochlorite acid fuming 37%	Emsure® ACS	Merck
In solution	In ICP standard, 1000 mg/L In	Certipure®	Merck
ICP-MS standard	ICP-MS calibr. stand. 4, 10 mg/L	Prolabo®	VWR

2.5. Analysis of Sample Digests

Liquid measurements were performed on the ICP-MS with standard mode settings as shown in Table 6. Aqueous standard solutions were prepared before each measurement. To cover a concentration range from 0 ppb to 100ppb boron, five standards of different boron concentration within that range were processed according to 2.4, whereas the lowest concentration standard was always 0 ppb (blank). After doing so, standards were measured to set up a calibration function for the evaluation of the boron concentration in digested vacuum sintered sample solutions.

In order to ensure precision and accuracy of the experiment, concentration of boron in sample digests had to be adjusted to the concentration range of the calibration function of aqueous standard solutions. Hence linearity of data points could be assured. For that matter, five replicates of five sample digests of different boron concentration (within the range of 0ppb to 100ppb) were processed as described in 2.4 and, again, measured with the ICP-MS in liquid standard mode.

2.6. LA-ICP-MS Investigations

In the current thesis three different approaches for the quantification of boron were established and optimized. Depending on the issue of said quantification one particular approach has proven to be more suitable than the others. In the following those three methods, in particular for the evaluation of total boron concentration, the boron depth-profile and lateral boron distribution (imaging) will be presented.

2.6.1. Data Processing

As mentioned in paragraph 2.3, thermo scientific Qtegra™ version 2.2.1465.24 was used as the software for data acquisition. This software provides a tool which allows the controller to set arbitrary time frames for data processing. These frames are called regions. Within this region, the average signal intensity for each element detected is calculated.

Figure 17 shows an exemplary set up of such regions for the data analysis of an intensity/time profile of an investigated sample. Regions are adjusted to cover the time frame during which a sample originating analyte signal is detected. Also, to get rid of the background signal, a region of the exact same time frame is set for the gas blank and subtracted from all other regions. It is up to the controller to adjust size and amount of those regions to optimize data evaluation and it varies to a certain degree depending upon the method and goal of investigation. In this work, different set ups were applied for calculations. In the following, they are described for each of the methods developed which differ in the approach for boron quantification.
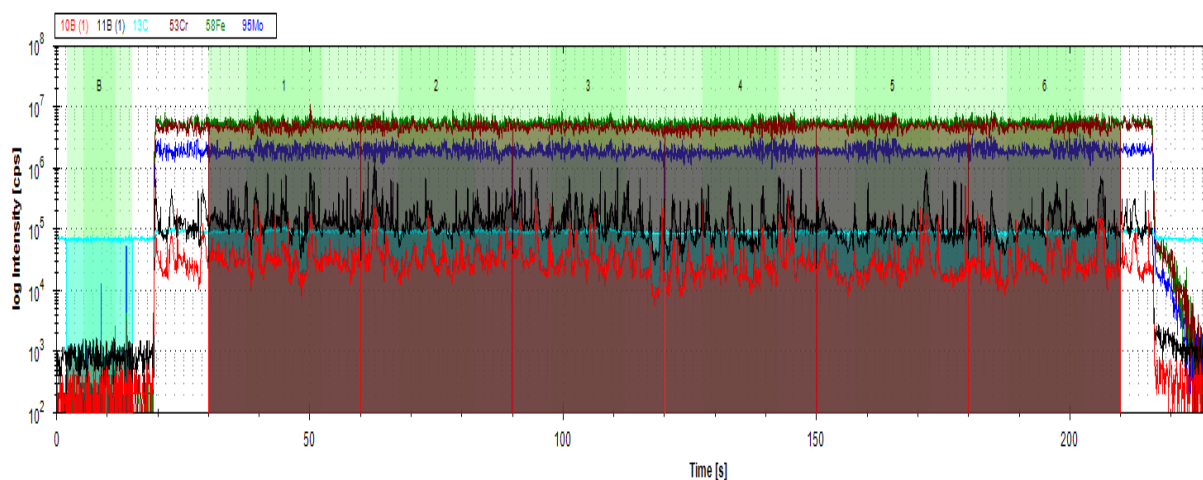
Figure 17 - exemplary set up of regions for data analysis performed with LA-ICP-MS; B= gas blank region; 1-6=regions for calculation of analyte signal

2.6.2. Measurement of Total Boron Concentration in Samples

This method was developed for optimizing measurements of the total boron concentration in samples sintered under vacuum conditions or in argon and hydrogen atmosphere, respectively.

For measurements, embedded sample bodies were loaded into the sample chamber and laser settings were adjusted as in Table 9. Evaluation of the total boron concentration in samples of different contents of analyte was established using line scans. Figure 18 shows an ablation pattern of such line scan applied onto the surface of sample cross section. The scan direction is performed in serpentine lines whereas the scan direction is reversed and the ablation pattern repeated when hitting the endpoint of said pattern. To assure representative and valid measurement 5 line scans per sample were performed and the average concentration was then evaluated. One line scan was centered on the sample surface and the other four of them positioned around it for the purpose of uniformity. This particular line scan pattern is presented in Figure 19. For calculations, several (6-7) so called regions were placed for each pattern. Applying regions enables the determination of an average intensity merit (counts) for certain analyte in a given time frame. Gas-blank was subtracted for each region and the average of these regions was calculated. After that the average of the average of the 5 ablated patterns was calculated and used for the calibration. Before each measurement pre ablation was performed according to Table 9.
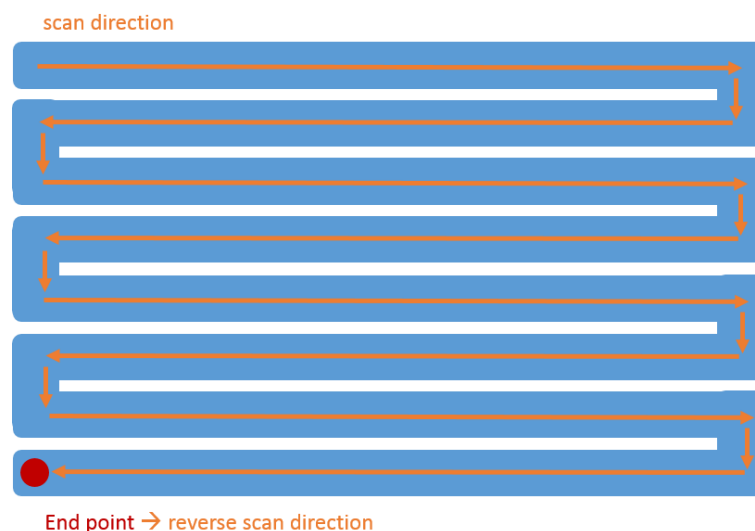
Figure 18 - schematic ablation pattern when performing line scan; scan direction is reversed after hitting end point

Table 9 - laser settings applied when measuring boron vacuum sintered samples

Parameter	Unit	Standard settings	Pre ablation settings
Laser beam diameter	µm	200	200
Repetition rate	Hz	10	10
Fluency	J/cm^2	5.71	3.42
Scan speed	µm/s	300	300
Carrier gas flow (He)	L/min	0.5	0.5
He/Ar-gas flow	L/min	0.5/0.98	0.5/0.98
Time per scan	min	4	-

Figure 19 - schematic example of ablation pattern used for measuring total boron concentration; for evaluation of boron concentration average value of 5 line scans was calculated

2.6.3. Measurement of Lateral Boron Concentration (Imaging)

Imaging was performed on embedded cross sections of argon and hydrogen sintered specimen. For calculations of the lateral boron concentration line scans were used and laser settings adjusted as in Table 10. Pre ablation was performed to enable better surface homogeneity. The investigated area was set to be 1 mm^2.

Analysis and evaluation was done with Imagelab (©2013 Epina GmbH; v. 0.4).

scan direction

area of ablation: 1mm^2
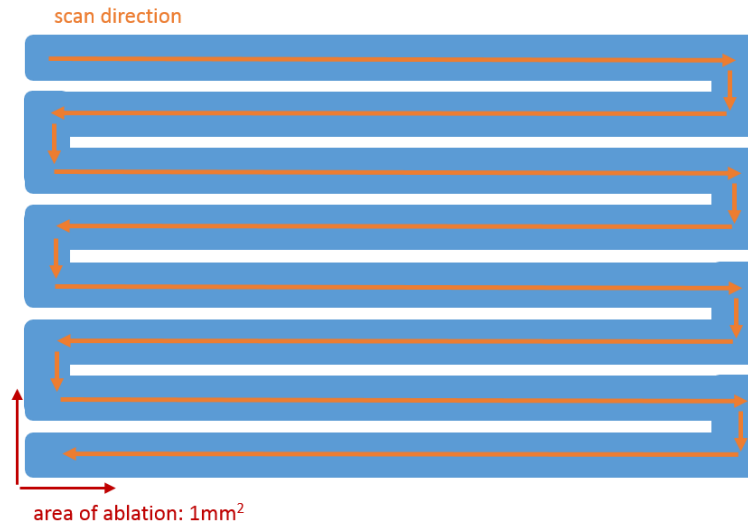
Figure 20 - schematic ablation pattern used for imaging

Table 10 - laser settings applied when performing lateral boron measurements in Ar- and H$_2$ - sintered samples

Parameter	Unit	Standard settings
Laser beam diameter	μm	20
Repetition rate	Hz	10
Fluency	J/cm^2	5.71
Scan speed	μm/s	10
Carrier gas flow (He)	L/min	0.5
He/Ar - gas flow	L/min	0.5/0.98

2.6.4. Measurement of Boron Depth Profile

Investigations were performed on the cross sections of the sample bodies. For the determination of the depth distribution of boron in argon and hydrogen sintered samples a method using line scans has been developed. For that matter line scans of a particular laser beam diameter were placed next to each other on the face side of the specimen starting with the outermost one which was closest to the sample surface continuing towards the inside, aiming for a scan pattern which is representative of the depth distribution of boron in the samples. Each line was scanned four times to increase recording time per line scan. Also each repetition was set to be one region leading to a total of four regions per line scan. For data analysis the average of those 4 regions was determined and its standard deviation was calculated. The described line scan ablation pattern is graphically displayed in Figure 21.
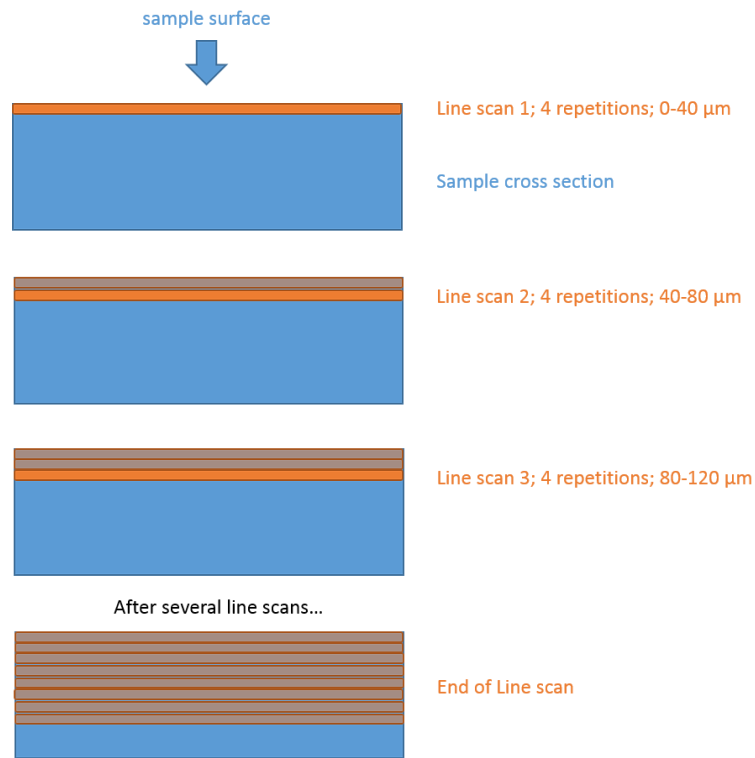
Figure 21 - illustration of line scan pattern used for determination of boron depth profile

Laser settings used for measuring the boron depth profile are presented in Table 11. Settings for pre ablation are shown as well in the following table.

Table 11 - laser settings applied when measuring depth profile of boron in Ar- and H_2-sintered samples

Parameter	Unit	Standard settings	Pre ablation settings
Laser beam diameter	μm	40	40
Repetition rate	Hz	10	10
Fluency	J/cm^2	5.71	3.42
Scan speed	μm/s	300	300
Carrier gas flow (He)	L/min	0.5	0.5
He/Ar - gas flow	L/min	0.5/0.98	0.5/0.98
Time per scan	min	2	-

Furthermore, investigations regarding differences in boron content between sample surface and bulk were performed in order to acquire more information about the distribution of boron in a vertical manner. Therefore, quantification of boron was carried out on sample cross sections and sample surfaces which were representative of the bulk and surface of the PM-

steel specimen, respectively. For surface characterization, fractions of the sintered samples have been mounted in Bakelite so that the outer surface of the specimen could be studied. Those mounted sample bodies (cross sections and sample surfaces) were analyzed via LA-ICP-MS whereby line scans were performed, see Table 12. Other than the method for quantifying total boron concentration in solid samples, results are based on calculations of 4 line scans per sample. Each line scan is divided into 7 regions accounting for 4min scan time in total. Concerning bulk measurements, areas of line scans were positioned inward sample cross sections to exclusively provide bulk analysis.

Table 12 - laser settings applied for determining differences in boron concentration between surface and bulk of argon and hydrogen sintered samples.

Parameter	Unit	Standard settings	Pre ablation settings
Laser beam diameter	μm	200	200
Repetition rate	Hz	10	10
Fluency	J/cm^2	5.71	3.42
Scan speed	μm/s	300	300
Carrier gas flow	L/min	0.5	0.5
He/Ar gas flow	L/min	0.5/0.98	0.5/0.98
Time per scan	min	4	-

3. Results and Discussion

In this section results of performed experiments will be presented and discussed.

In the first part, data concerning sample characterization in terms of mechanical, physical and metallographic properties will be presented and their relation to boron content in samples determined.

Second, quantification of boron using LA-ICP-MS and methods established for measuring depth profile and lateral boron concentration will be discussed and evaluated. Also results of said measurements will be reported.

All limits of detection in this chapter were calculated using Equation 7.

Equation 7 - Limit of Detection

$$LOD = \frac{(bl_{av} - 3 * \sigma) - d}{k}$$

bl_{av}... Average of blank measurements
σ... Standard deviation of blank measurements
d... Intercept of calibration line
k... Slope of calibration line

3.1. Physical and Mechanical Properties

Physical and mechanical properties of Ar- and H_2-sintered samples are shown in Table 13.

Table 13 - mechanical and physical properties of Ar- and H_2-sintered samples with increasing concentrations of boron

Sample name	B concentration [wt.%]	Green Density [g/cm^3]	Sintered Density [g/cm^3]	Vickers' Hardness HV 30	Microhardness HV$_{m0.1}$	Impact energy [J/cm^2]
0 - Ar	0		7.07	111	340	23
0 - H$_2$	0	6.83	7.11	108	333	19
750 - Ar	0.075		7.26	174	383	14
750 - H$_2$	0.075	6.76	7.27	152	416	8.5
1500 - Ar	0.15		7.38	203	411	6.5
1500 - H$_2$	0.15	6.72	7.54	248	408	4.0
3000 - Ar	0.3		7.35	175	412	2.3
3000 - H$_2$	0.3	6.72	7.77	299	404	2.5
6000 - Ar	0.6		7.40	198	383	1.5
6000 - H$_2$	0.6	6.66	7.74	315	374	1.5

Bulk densities of samples in pre-sintered and sintered states are shown in Table 14 and Table 15.

Table 14 - Average green density of green bodies with increasing boron content; n=3

Boron conc. in sample [ppm]	Green density [g/cm^3]	STDEV [g/cm^3]
0	6.825	0.015
750	6.759	0.014
1500	6.720	0.007
3000	6.724	0.022
6000	6.655	0.026

Table 15 - Sintered densities of Ar- and H$_2$-sintered samples in comparison; n=1

Boron conc. in sample [ppm]	Argon sintered Sintered density [g/cm^3]	H$_2$ sintered Sintered density [g/cm^3]
0	7.07	7.11
750	7.26	7.27
1500	7.38	7.54
3000	7.35	7.77
6000	7.40	7.74

Results for green density and sintered density show that densification of Ar- and H$_2$- sintered samples occurred. Also, first assumptions which can be made regarding the effect of boron as an agent for activated sintering.

First, boron enhances densification in investigated samples both for argon and hydrogen as sintering gases. This consideration can be justified when comparing values for sintered density of non-boron-containing samples to the ones containing boron (samples 750-6000).

Second, densification increases with increasing content of boron from 750 to 6000pm for both samples sintered in argon and hydrogen atmosphere (Table 15). In fact, even for samples with the smallest boron concentration (750ppm) legitimate increase in density is examined which is very interesting in technological terms.

Moreover, results in Table 15 additionally point out that there is an obvious contribution of the sintering gases on the level of densification of investigated samples. A comparison of data reveals that without exception samples sintered in hydrogen atmosphere show higher values in sintered density than the ones of samples sintered with argon. On top of that, the ratio of sintered densities increases with an increasing boron concentration. Figure 22 illustrates said relation.
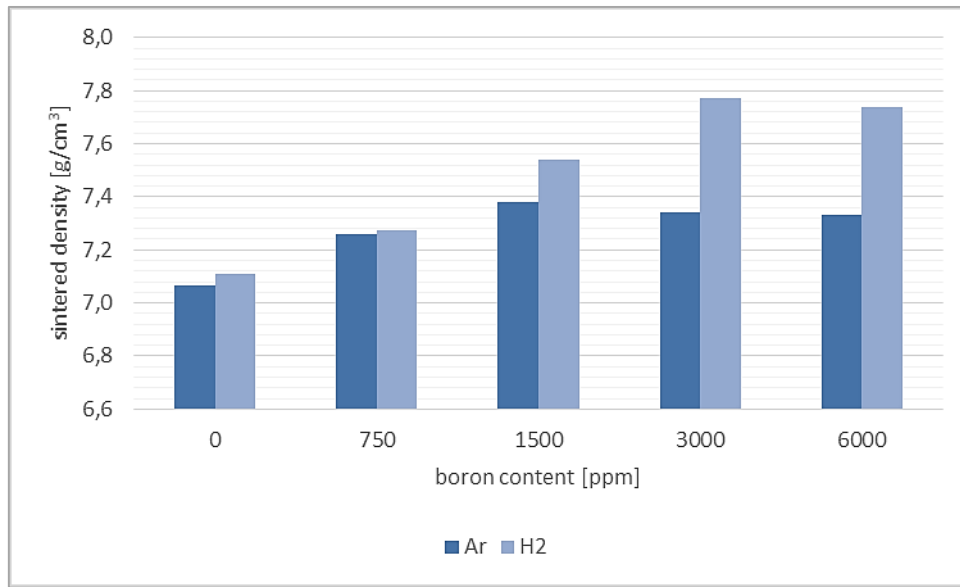
Figure 22 - sintered density of Ar- and H₂-sintered samples; n=1

Dilatometry data shows the same behavior in densification of investigated samples. The activating effect of the boron addition can be seen on the dilatometry graph in both atmospheres (Figure 23 and Figure 24). The black and the brown graph (6000ppm B and 3000ppm B, respectively) in the hydrogen sintered samples run into overflow, as the maximum shrinkage of the system (2500 µm) is reached and no further densification can be detected. The graphs again show that even a very small addition of boron already gives a noticeable effect on sintering. Certainly 6000ppm boron is too much, as both samples (argon and hydrogen) almost lost their shape due to the excessive amount of liquid phase formation. The sudden drop of the dilatometry curves at about 80min of time represents the transformation of the iron lattice in the sample. This particular transformation is a polymorph transition of α-Iron (Ferrite) to γ-Iron (Austenite). The iron lattice changes from body-centered- to face-centered cubic causing a decrease in volume or increase in density which can be recognized as said sudden shrinkage of samples. Reconversion to α-Iron takes place at about 270min of time as shown in Figure 23 and Figure 24.

Boron acts as a stabilizer for the austenitic structure, which means it enhances the solubility of carbon in the iron lattice. Hence, there is a noticeable shift in the α-γ conversion and γ-α reconversion to lower temperatures when comparing samples without boron (0ppm) to the ones containing some, for both argon- and hydrogen sintering atmospheres. However, that shift doesn't change for samples with higher boron contents, since there is an increased amount of non-soluble boron which cannot contribute to the stabilization of that γ-phase anymore.
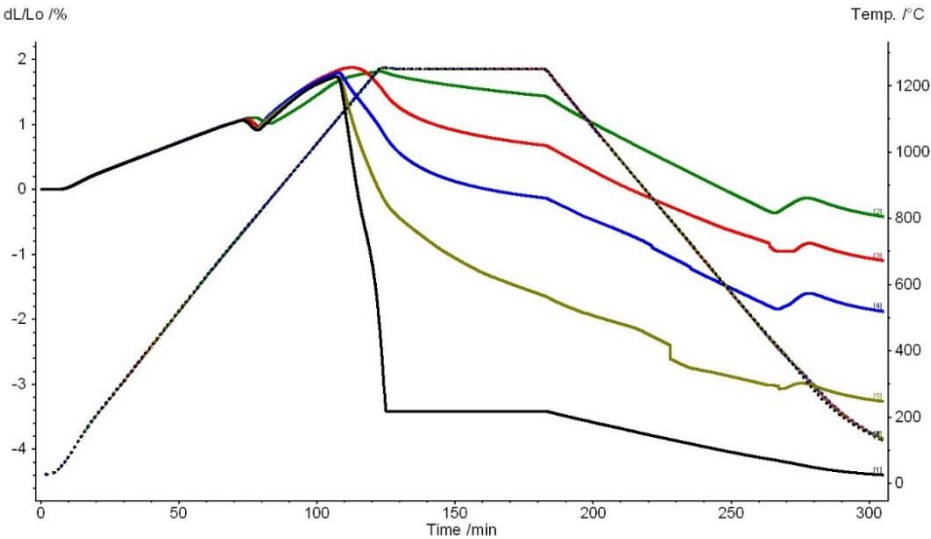
Figure 23 - Dilatometry graphs of Ar-sintered samples with different amounts of boron; 1250°C 60 min, 10 K/min (green=no boron, red=750ppm, blue=1500ppm, brown=3000ppm and black=6000ppm boron; dotted line=temperature profile of sintering)
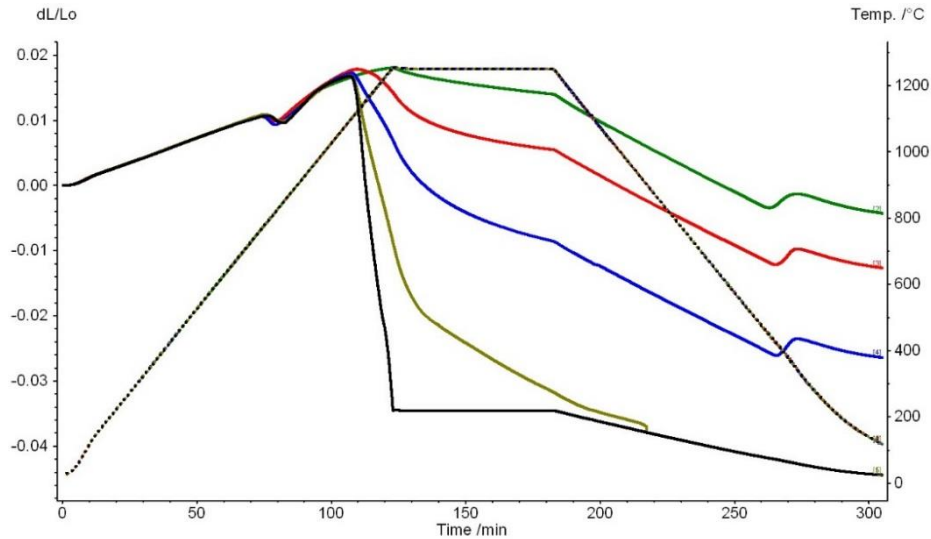
Figure 24 - Dilatometry graphs of H₂-sintered samples with different amounts of boron; 1250°C 60 min, 10 K/min (green=no boron, red=750ppm, blue=1500ppm, brown=3000ppm and black=6000ppm boron; dotted line=temperature profile of sintering)

Considering much lower merits of sintered density of argon-sintered samples compared to the ones of specimen sintered with hydrogen (Table 15) it seems like there is a limiting threshold for densification. That being said, it is obvious that argon as sintering gas is the main contributor to mentioned circumstance. For the samples sintered in argon, densification stopped because of the formation of large gas-filled pores, which cannot be found in the samples sintered in hydrogen. Micrographs of sample surfaces sintered in different atmospheres evidentially show mentioned behavior of argon in bulk material (Figure 25).
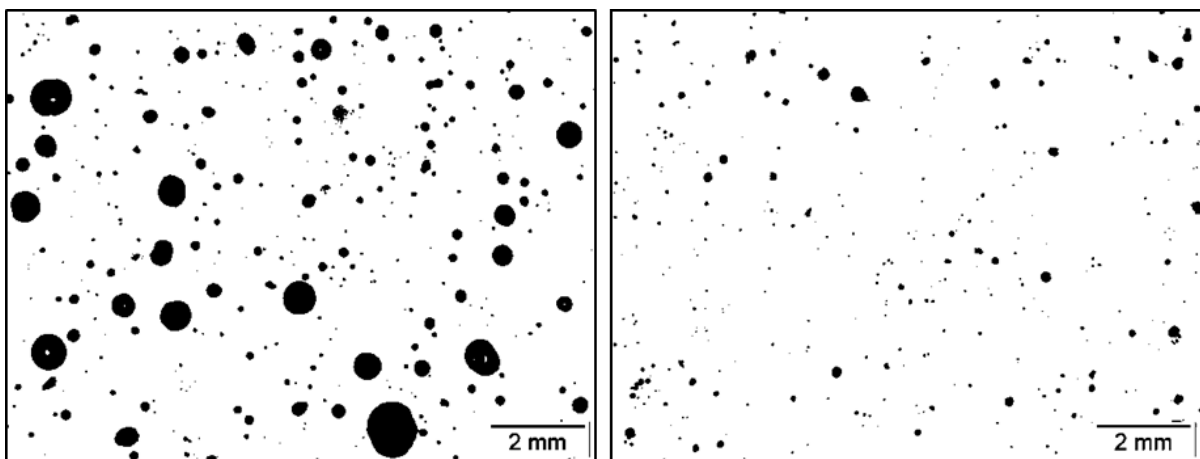
Figure 25 - Unetched microstructure of samples with 3000ppm boron sintered in different atmospheres; left: argon, right: hydrogen

Results for macro hardness are reported in Table 16 and Table 17. As expected, the hardness of samples increases with an increasing boron content. Even the smallest amounts of the sintering agent result in a drastic improvement in hardness of the material (750ppm) and densification, as mentioned in the previous paragraph. What is more, specimen sintered with hydrogen gas exhibit higher hardness than those sintered with argon gas particularly for higher boron contents. Figure 26 illustrates the mentioned circumstances.

Table 16 - Average Vickers' hardness of Ar-sintered samples; HV 30; n=5

Sample name	Vickers' hardness HV 30	STDEV HV 30
0-Ar	111	2
750-Ar	174	13
1500-Ar	203	14
3000-Ar	175	11
6000-Ar	198	7

Table 17 - Average Vickers' hardness of H_2-sintered samples; HV 30; n=5

Sample name	Vickers' hardness HV 30	STDEV HV 30
0-H2	108	4
750-H2	152	6
1500-H2	248	32
3000-H2	299	10
6000-H2	315	14

Regarding low merits of hardness for argon sintered specimen, it has to be kept in mind that results established by using the method described in chapter 2.2.3. for measuring Vickers' hardness, do not exclude porosity of the investigated material from calculations. Therefore, there is high porosity in argon sintered samples due to gas retardation in sample bodies which is a great contributor to low hardness of specimen.
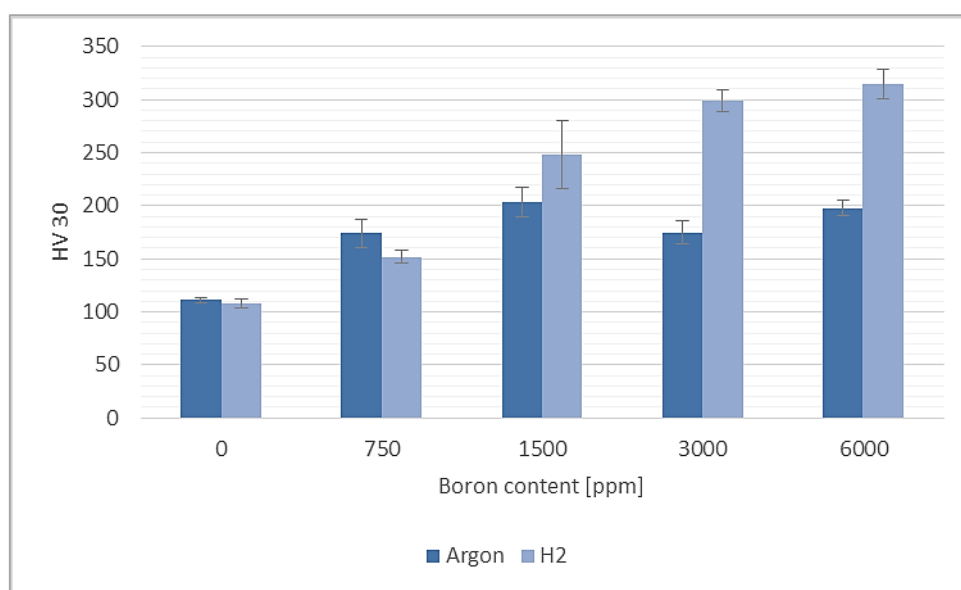
Figure 26 - Average Vickers' Hardness of Ar and H_2-sintered samples; HV30; n=5

Obviously hardness and density of sample material follow the same trend when talking about the impact of increasing boron concentration in analyzed specimen. In general one can say that for a material of a given composition and microstructure, there is a direct relationship between density and hardness. The lower the density, the lower its apparent hardness will

be.[53] That being said one can argue that both properties increase with increasing boron content. This relationship is shown in Figure 27.
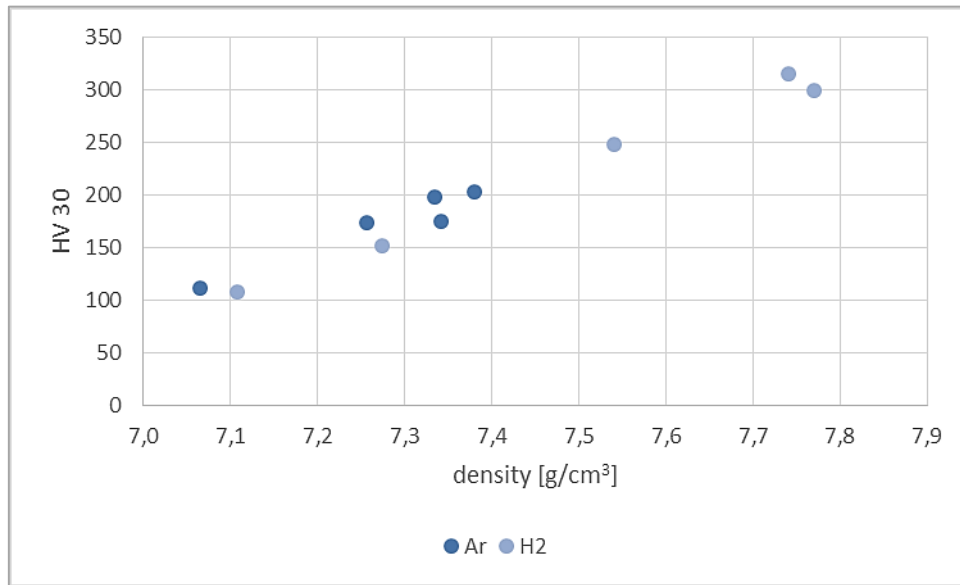
Figure 27 - Correlation between Vickers' hardness and sintered density of Ar- and H$_2$-sintered samples; higher sintered density leads to higher hardness determined as Vickers' hardness in this particular case

Results for impact toughness are shown graphically in Figure 28. The impact of energy should only be taken as an indicator of embrittlement, as only one sample of each composition was measured. Higher contents of boron lead to increased amounts of eutectic phase. Consequently, the amount of segregated phase at grain boundaries increase as well which results in the embrittlement of the material.
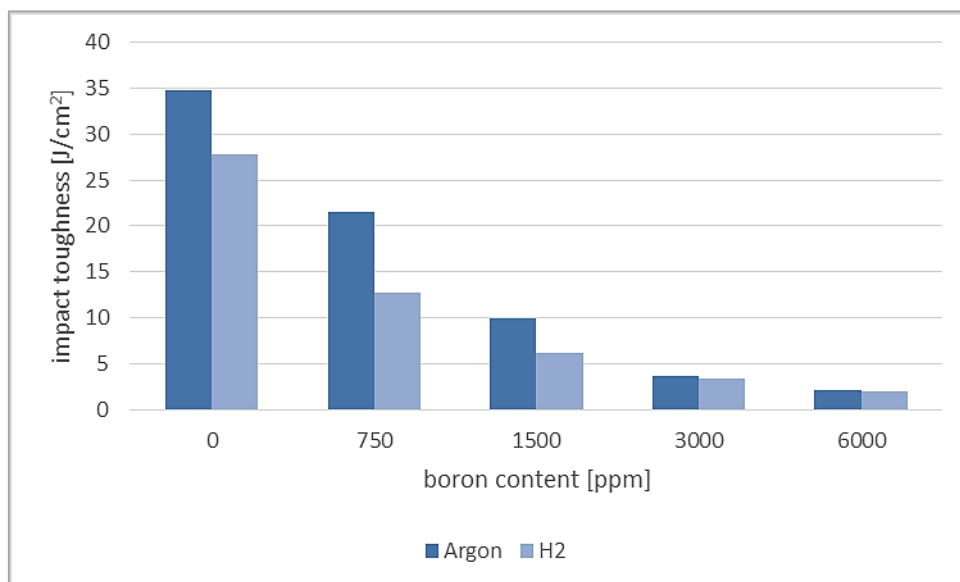
Figure 28 - impact toughness of Ar- and H$_2$-sintered samples; n=1

---

[53] (ASTM, 2012)

Micro hardness was evaluated both for argon and hydrogen sintered samples for all boron concentrations. Since the intender is very small in size investigation of different phases or features of samples was enabled. Therefore, micro hardness of grains and boron rich grain boundaries were determined and compared. The measurement of grain boundaries (segregations) was only possible for samples containing the highest amount of boron (6000ppm) since they were the only specimen where the area of the solidified eutectic phase at grain boundaries was large enough to be examined without having getting contributions of surroundings hit by the intender. Results are shown in Table 18 and Table 19.

As mentioned before micro hardness was measured within the core of the metallic matrix mostly, rather than in the solidified eutectic for each sample where microhardness > 800 $HVm0.1$ was measured. It is interesting that even the lowest content of boron resulted in significant densification and higher hardness. Micro hardness especially did not reach higher values at higher boron contents which proves the low solubility of boron in the iron rich alloy matrix. Especially high merits of microhardness measured at grain boundaries validate the assumption of a hard, brittle eutectic phase segregated at grain boundaries and will be testified later on.

Table 18 - Results of Microhardness of samples sintered in argon; $HV_{m0,1}$

Microhardness $HV_{m0,1}$ measured in…

Sample name	grain	grain boundary
0-Ar	340 ± 42	-
750-Ar	383 ± 26	-
1500-Ar	411 ± 17	-
3000-Ar	412 ± 117	-
6000-Ar	383 ± 6	718 ± 36

Table 19 - Results of Microhardness of samples sintered in hydrogen; $HV_{m0,1}$

	Microhardness $HV_{m0,1}$ measured in…	
Sample name	grain	grain boundary
0-H2	333 ± 24	-
750-H2	416 ± 24	-
1500-H2	408 ± 13	-
3000-H2	404 ± 72	-
6000-H2	374 ± 4	857 ± 57

3.2.   Metallographic Examination

In order to talk about material properties as well as to justify and understand the behavior of investigated material or specimen, it is very reasonable to look at micrographs of metallographically prepared surfaces of sample cross sections.

Figure 29 to Figure 33 show micrographs of unetched surfaces of sample cross sections. As discussed in the previous paragraph pictures show increasing porosity with higher boron content for argon sintered samples. Moreover the shape of pores changes from elongated and angular to circular ("bubble"-like) as the amount of liquid eutectic phase increases with higher boron concentration in specimen. For hydrogen sintered samples pores also become smaller in size and the degree as densification increases. Especially samples with 6000ppm boron (Figure 33) exhibit exceeded eutectic phase segregation at grain boundaries forming a brittle network, which is ultimately the reason for low merits of impact toughness. The impact of the boron content on the embrittlement of the samples is presented in Figure 28.
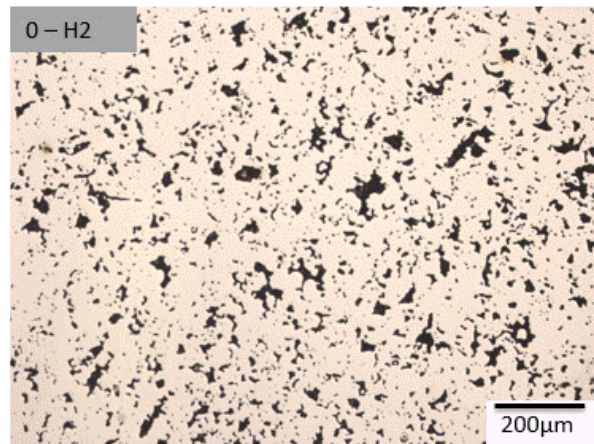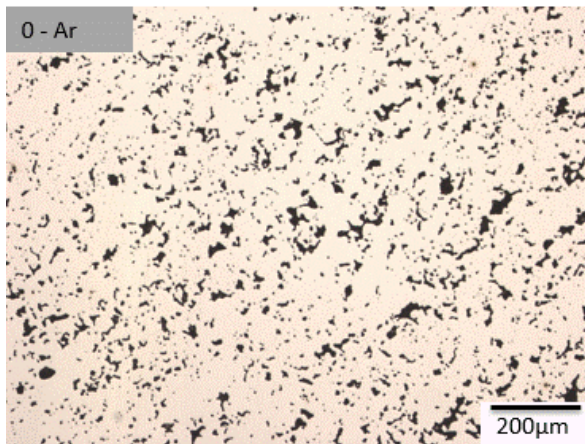
Figure 29 - Unetched surface of samples containing no boron sintered in Ar (left) and H_2 (right); cross-section of sample
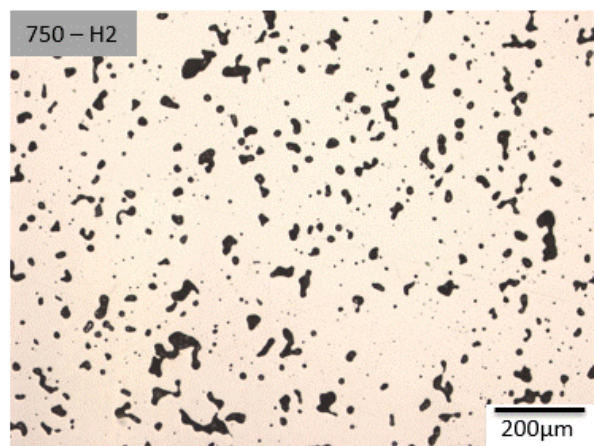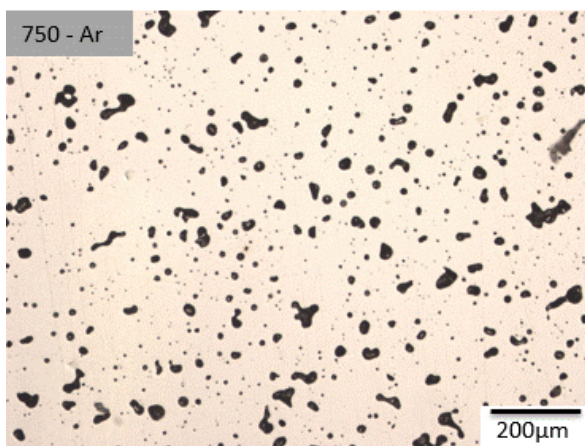
Figure 30 - Unetched surface of samples containing 750ppm boron sintered in Ar (left) and H_2 (right); cross-section of sample
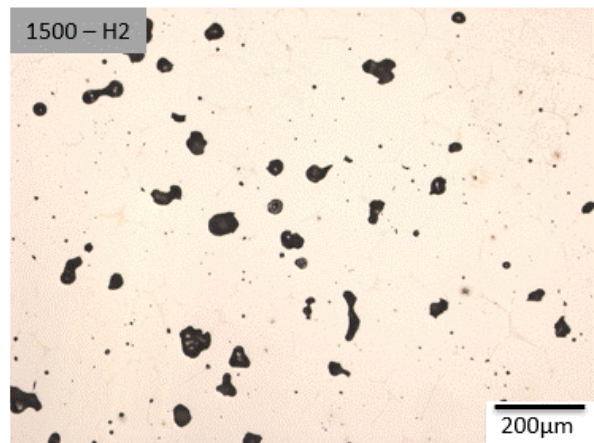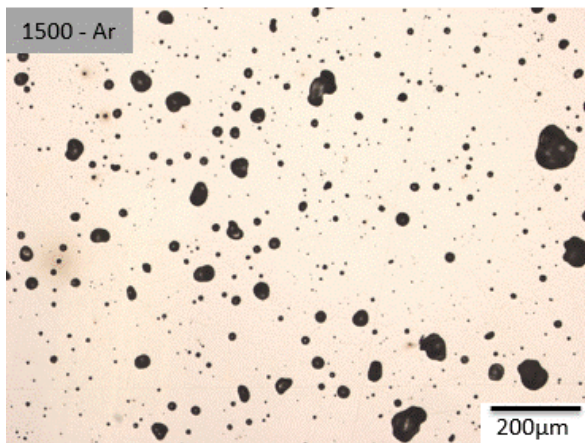
Figure 31 - Unetched surface of samples containing 1500ppm boron sintered in Ar (left) and H_2 (right); cross-section of sample
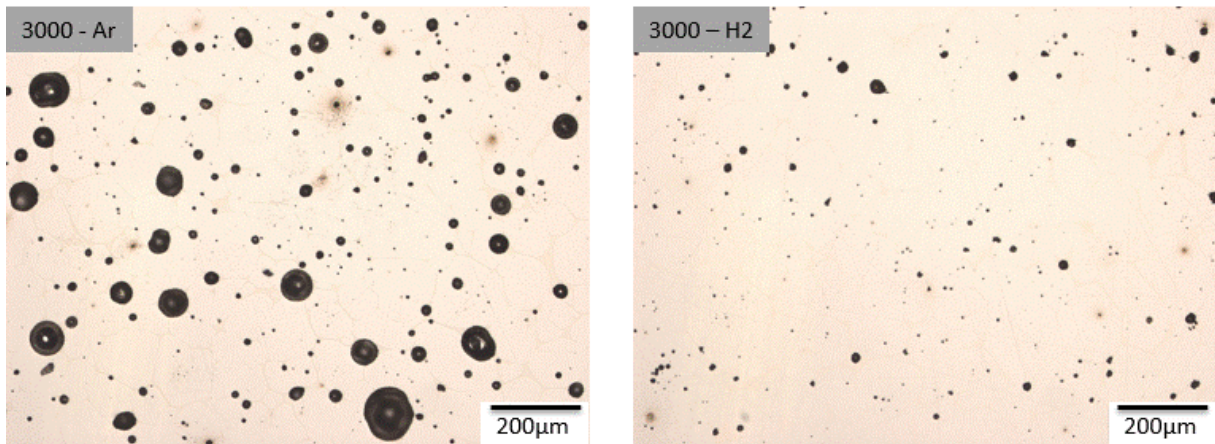
Figure 32 - Unetched surface of samples containing 3000ppm boron sintered in Ar (left) and H₂ (right); cross-section of sample
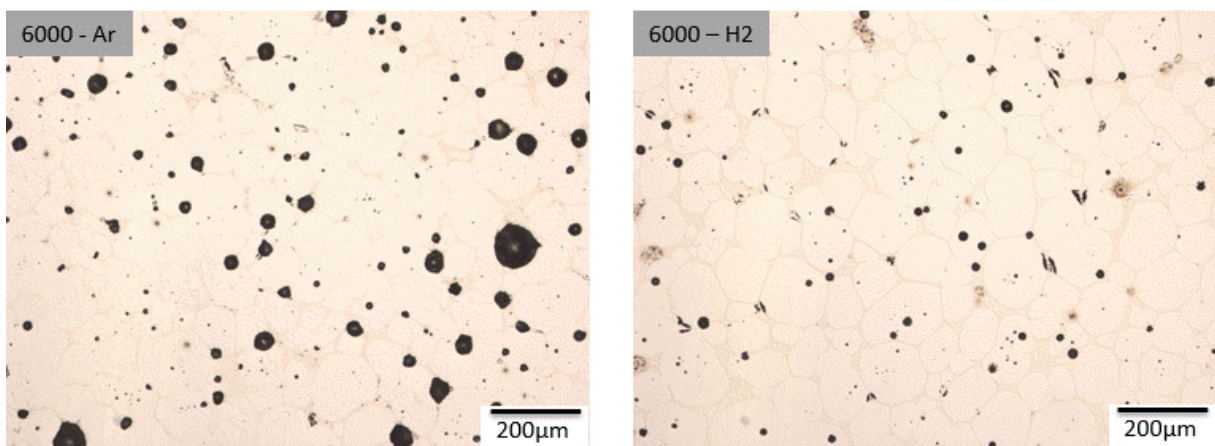
Figure 33 - Unetched surface of samples containing 6000ppm boron sintered in Ar (left) and H₂ (right); cross-section of sample

For further investigation, SEM images of fracture surfaces of samples were taken. The reason for the embrittlement can be seen on the micrographs in Figure 34, Figure 35 and Figure 36, which show a dramatic change in the fracture mechanism. The boron-free material only shows a ductile fracture and an addition of only 0.075 w% boron leads to a brittle fracture. The higher the amount of boron, the fewer ductile dimples can be found on the broken surfaces, and the more the fracture mechanism changes from a transgranular to an intergranular fracture.
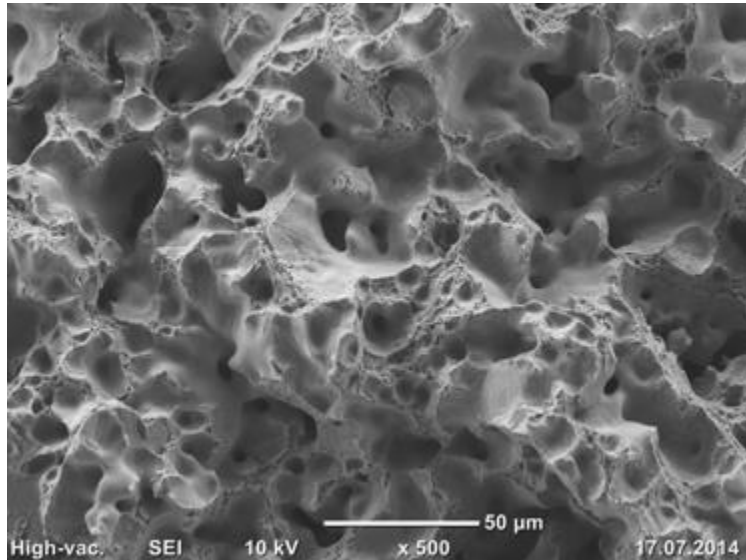
Figure 34 - Fracture surface of sample containing no boron; sintered in hydrogen; SEM
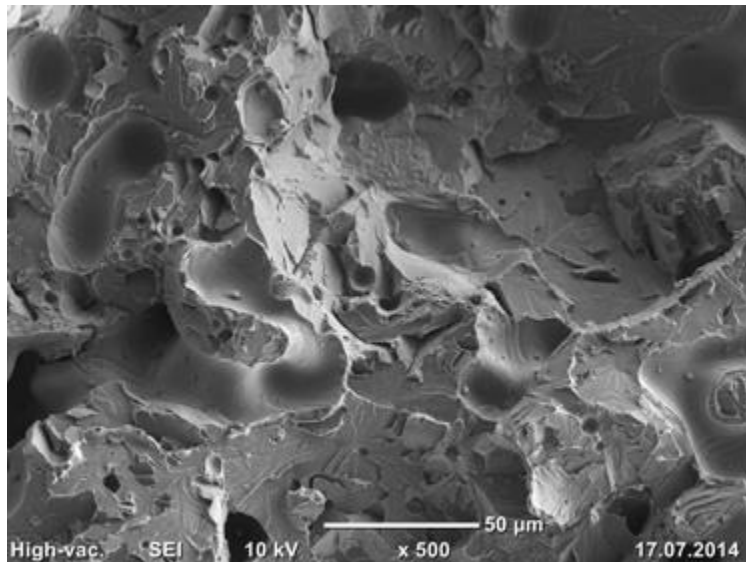
Figure 35 - Fracture surface of sample with 750ppm boron; sintered in hydrogen; SEM
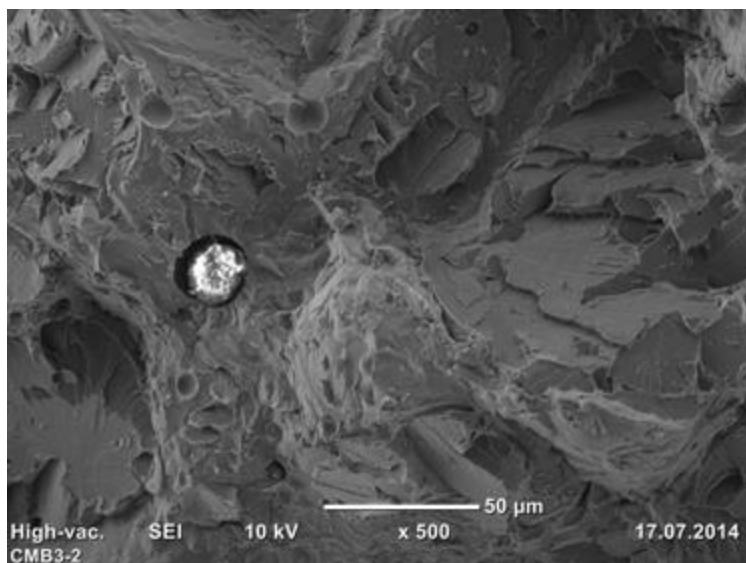
Figure 36 - Fracture surface of sample with 3000ppm boron; sintered in hydrogen; SEM

Figure 37 to Figure 41 show images taken of etched surfaces of argon and hydrogen sintered samples ranked in the order of the boron quantity. The amount of eutectic phase (white appearance) solidified at grain boundaries increases as boron concentration is raised, which can be examined when looking at said images. This leads to the formation of a network of eutectic, solidified phase which becomes more evident at high boron concentrations (Figure 39, Figure 40 and Figure 41). The hard but brittle phase promotes crack formation and crack propagation along the eutectic constituent.[54] Therefore impact toughness decreases drastically.
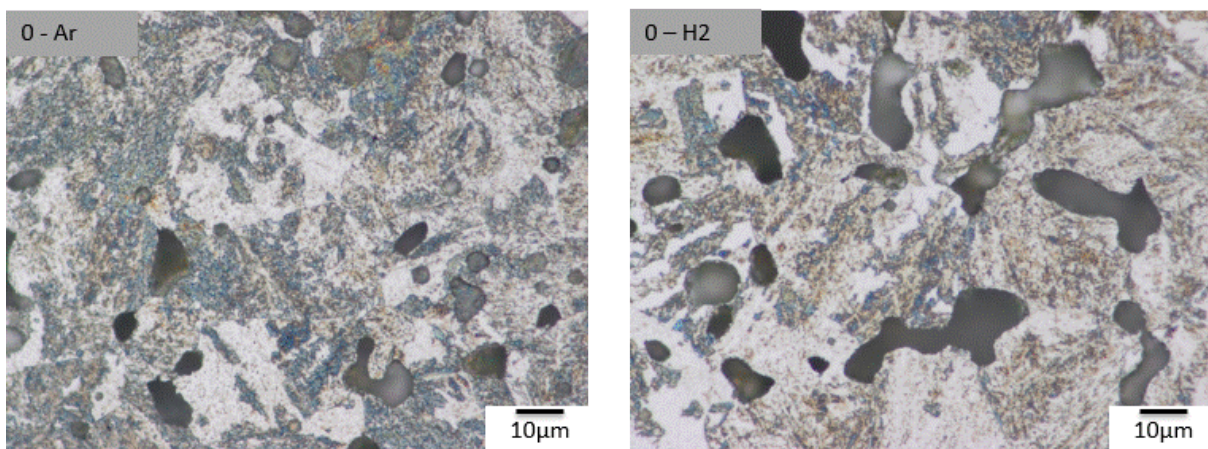
Figure 37 - Etched surface of samples containing no boron sintered in Ar (left) and H$_2$ (right); cross-section of sample
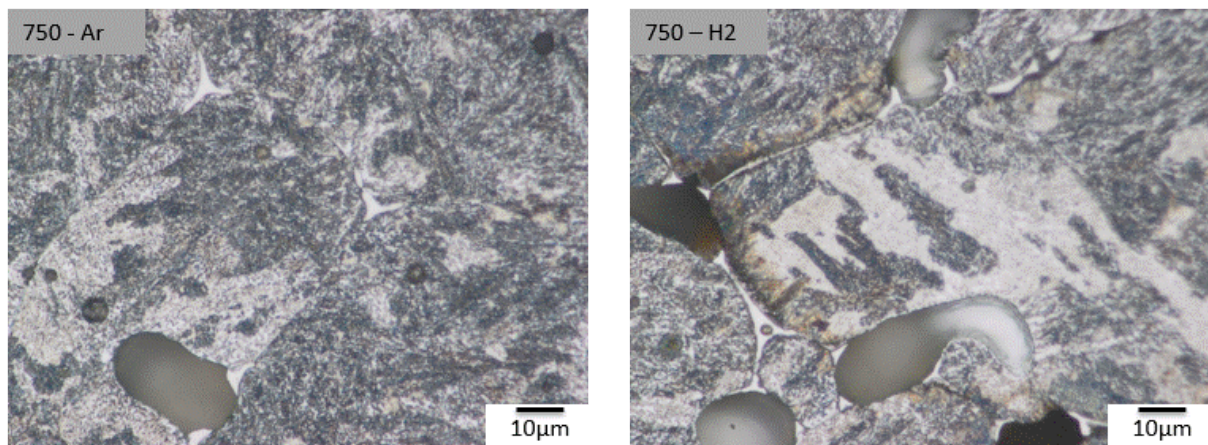
Figure 38 - Etched surface of samples containing 750ppm boron sintered in Ar (left) and H$_2$ (right); cross-section of sample

---

[54] (Kazior, 2002)
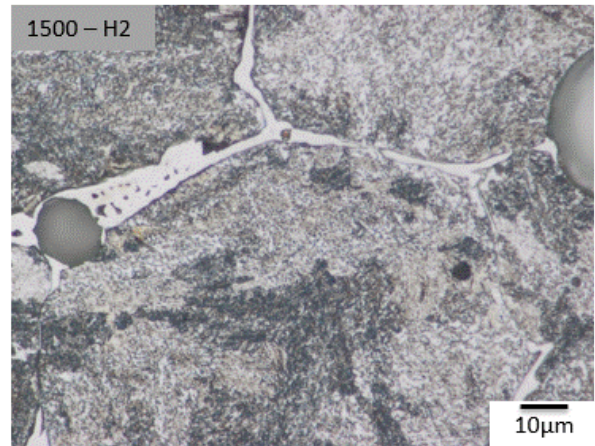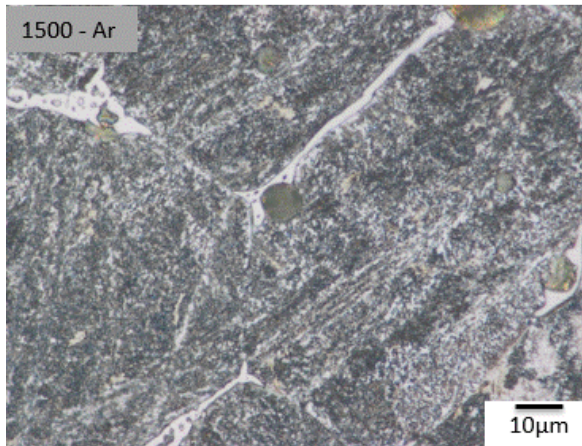
Figure 39 - Etched surface of samples containing 1500ppm boron sintered in Ar (left) and H_2 (right); cross-section of sample
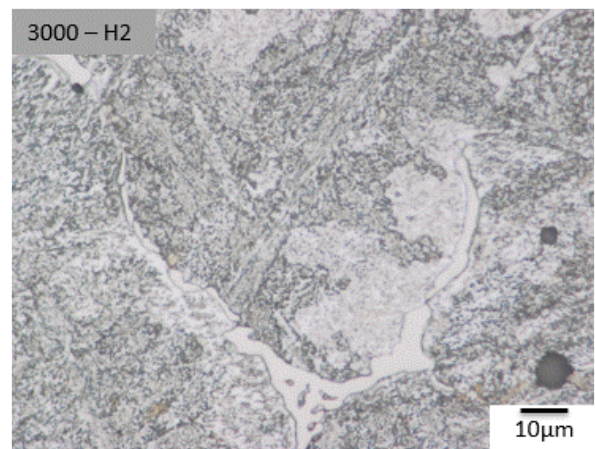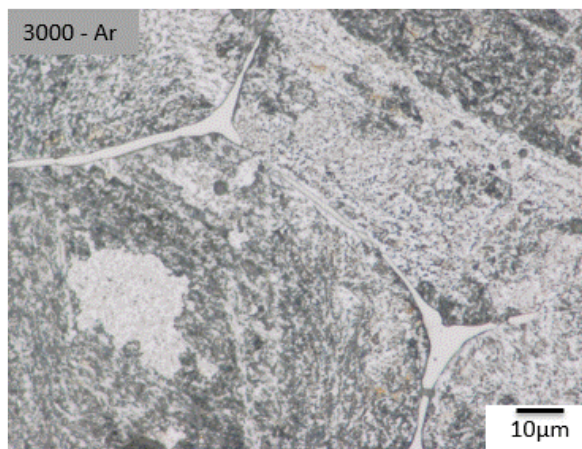
Figure 40 - Etched surface of samples containing 3000ppm boron sintered in Ar (left) and H_2 (right); cross-section of sample
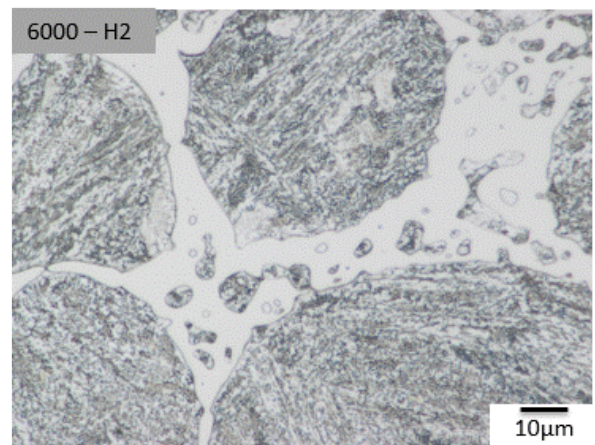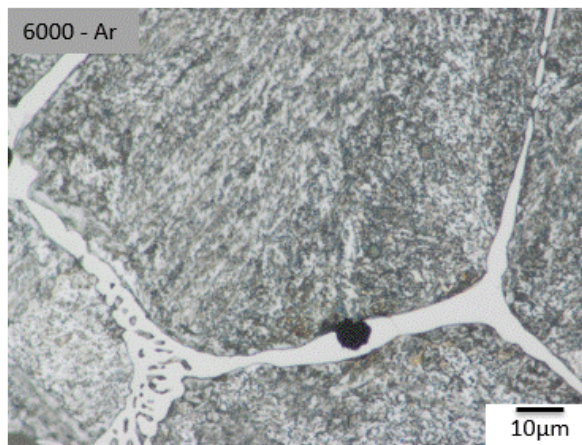
Figure 41 - Etched surface of samples containing 6000ppm boron sintered in Ar (left) and H_2 (right); cross-section of sample

3.3. (LA)-ICP-MS Measurements, Method Development and Evaluation

Quantitative measurement of boron in PM-samples required the development of new methods for an effective, reproducible and valid analysis. Also, in order to use LA-ICP-MS for quantitative analysis a calibration had to be developed, as no reference material was available. The preparation of samples and standards and the optimization of measuring parameters in LA-ICP-MS caused obstacles which had to be overcome.

As no certified reference material for boron was available, in-house solid standards had to be prepared to enable analysis. In order to determine concentration of boron in those standards, ICP-MS analysis of aqueous standards and digested standards was carried out. After that evaluation, solid standards were measured via LA-ICP-MS and a calibration function was set up allowing method development for the quantification of boron in argon and hydrogen sintered samples.

In the following, different approaches for measuring boron concentration laterally and in depth will be presented. Also the previously mentioned methods will be evaluated by discussing measurement results.

3.3.1. Liquid Measurements

First, measurements of liquid samples were performed on iCAP Q, ICP-MS in order to set up a calibration function enabling quantification of boron in investigated steel samples via LA-ICP-MS. Both isotopes, namely ^{10}B and ^{11}B, were measured and quantified. Since calibration functions for both isotopes showed quite similar residues (a little better for ^{10}B) for both isotopes the decision was made to consider ^{10}B isotope for all further calculations.

Calibration was established using standard solutions which were processed in accordance with 2.5. and measured in standard-mode as described in Table 6. The results of this measurement are illustrated in Figure 42.

f(x) = b*x + a				
Parameter	Value	Confidence Delta at 90%	StdErr	Rel. StdErr [%]
b	2,234.421	+/-36.099	22.042	0.986
a	2,546.098	+/-1,952.093	1,191.972	46.816
R^2	1.000			
BEC	1.139 ppb			
IDL(LOD)	0.032 ppb			
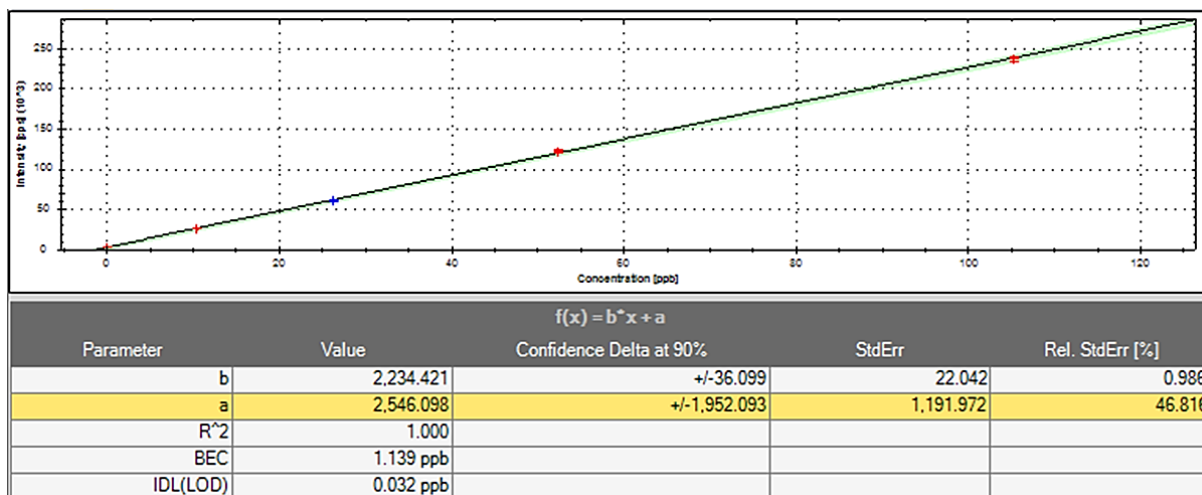
Figure 42 - calibration function of ^{10}B measured in calibration standards (2.5.)

Measured ^{10}B concentrations of calibration standards match with the calculated ones and show high precision (low standard deviation). Moreover, the calibration function intersect with the origin, concluding that there is little background signal during the measurement. Calibration with boron-standards between 0 to 100 ppb boron resulted in LOD of 0.032 ppb boron on ^{10}B.

Digested vacuum sintered samples which were diluted according to 2.4. were measured with the ICP-MS as well and their boron concentration was calculated using the calibration function of the standard solutions. Calculations are based on the measurement of five replicates of each standard to assure representative results.

*Table 20 - calculated concentration of ^{10}B in diluted vacuum sintered samples using the calibration function for standard solutions (2.5.) and taking dilution factor into consideration; calibration function: y = 2234.421*x+2546.098*

Nominal conc. [ppm]	measured ^{10}B [ppm]	STDEV [ppm]	RSD [%]
750	612	37	8
1500	1138	33	4
3000	2118	102	6
6000	5479	469	11

Merits in Table 20 show that there is a drastic difference between the expected concentration of boron in samples and measured values (second column). The calibration function (Figure 42) shows high precision and accuracy. Errors originating from the preparation process of standards can be ruled out since complete dissolution of all solid standards was achieved at all times. Also figures for standard deviation indicate high reproducibility of digestion processes and analysis implying that no mistakes were made in diluting standard solutions.

Nevertheless, systematic errors made during preparation of liquid standards and the process of weighting out powders, respectively, can't be ruled out.

One could argue that errors are deriving from the sintering process. However, the preparation process of solid standards, especially powder mixing, is most definitely the greatest contributor to that huge discrepancy between measured and nominal concentration. Considering the problems posed during sample homogenization, namely the agglomeration of particles and the bad mixing behavior between boron particles and the other constituents, this unsatisfying outcome is somewhat not unexpected. Nevertheless, further investigations have to be run to detect other sources of errors.

3.3.2. LA-ICP-MS Measurements of solid samples

In order to determine the boron concentration in solid samples sintered in argon and hydrogen atmosphere calibration function had to be set up. That being said, there was a need for a standard material which could be utilized to establish that calibration. Instead of purchasing a commercially available reference material, an ambitious objective was defined which was to manufacture self-made standards of different boron concentrations. This was a challenging task, since several important criterions had to be fulfilled:

First, a homogeneous distribution of boron in all standards had to be ensured. Efforts were made to process standards with proper homogeneity using argon as the sintering gas. The use of hydrogen for sintering was quickly dismissed since this particular gas is known for forming volatile boron-containing compounds which would eventually lead to the loss of analyte in the investigated bodies. Unfortunately, because of the formation of pores which were generated due to trapping of argon gas bubbles in the specimen bodies boron was not well distributed in standards sintered with argon gas either. Hence, other possibilities had to be taken into consideration. In order to achieve the aspirated homogeneous distribution of boron in standards, besides assuring no loss of boron through interaction with the sintering atmosphere and the formation of volatile compounds, vacuum conditions were applied during sintering. This was essential for processing sample standards which enable a valid and representative quantification of boron in the investigated specimen that were sintered in argon and hydrogen atmosphere. Vacuum sintered samples were processed as described in 2.1.

Second, sample preparation (particularly the powder mixing step) posed problems. Due to the complicated blending behavior of metals with non- or transition metals, homogenizing the ferrous powder with the crystalline boron was an issue. The application of ferroboron, as an alternative boron source to eliminate previously mentioned problems did not improve homogeneity, in fact it did quite the contrary: an agglomeration of constituents took place. Finally, satisfying homogeneity of powder constituents as well as the distribution of boron in the sample matrix was achieved by performing powder conditioning as described in 2.1.2.

Furthermore, the adjustment of measuring parameters was a major contributor to enhance the developed boron quantification methods. The sample ablation process in particular represented the most effective and efficient part for improvements in terms of method development. Since sample homogeneity could only be improved to a certain extent, laser ablation characteristics such as spot size, scan speed and scanned area presented easily accessible factors which could overcome the lack of homogeneity.

Adjusting scan speed was an important tool for improving boron quantification as mentioned in the previous paragraph. Slow ablation speed led to high inconsistencies in signal during measurement. Figure 43 shows such a line scan performed on a vacuum standard where logarithmic intensity of analytes is plotted against scan time. The green columns which are bounded by vertical red lines represent so called "regions" enabling the calculation of an average signal in that particular time frame (located in between those red lines). The red and black horizontal lines represent the intensity of ^{10}B and ^{11}B signal during measurement.
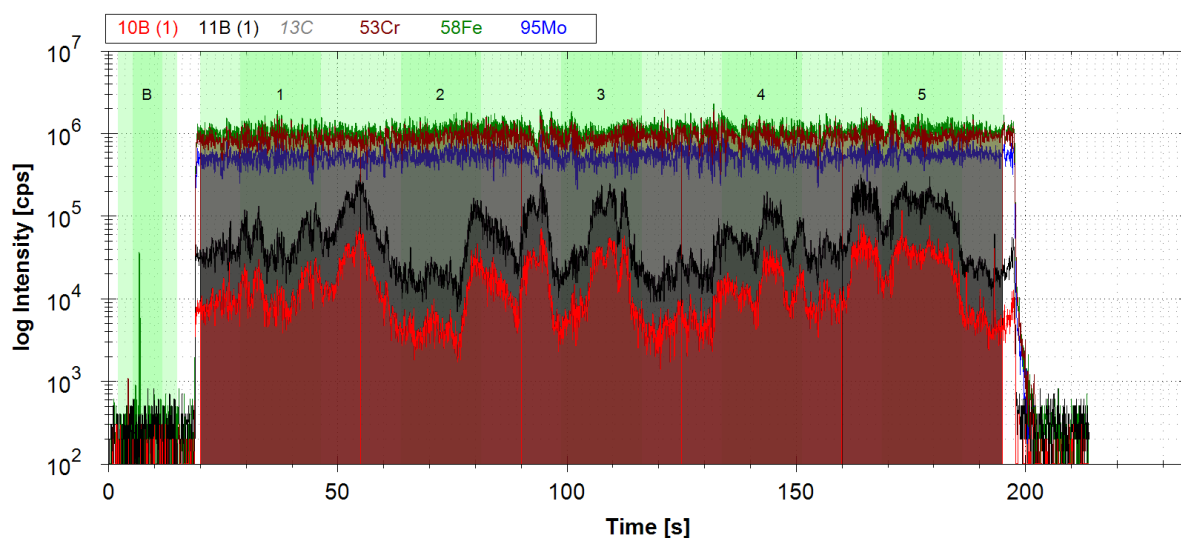
Figure 43 - 200 s line scan of 3000ppm vacuum standard with scan speed 100 μm/s showing high inconsistency in boron signal (10Hz, 200μm spot size, 5.71 J/cm², 0.5 l/min gas flow, 4mm² investigated area)

This previously described inconsistency in boron signal exists due to the limited uniformity of the analyte in the matrix, mainly because of the segregation of boron at grain boundaries. In other words, when the laser hits a grain, counts for boron (^{11}B as well as ^{10}B) drop off till boron rich grain boundary is ablated and signal rises almost instantly. By doing so, a sudden change in signal up to a factor of around 10 is observable. This is quite problematic since the overall measured (and calculated) average intensity of boron is strongly dependent on the uniformity of that element in the matrix. Hence, measurements are less reproducible and most notably not representative of the boron concentration in the investigated samples.

Besides all these issues mentioned in the previous paragraphs, the consistency of the analyte signal also suffered from several arbitrary, unpredictable disruption factors. Instrumental drifts, changes in ablation behavior, inconsistencies in particle transport and size heterogeneity of ablated particles were impacting signal variations and reducing the reproducibility of experiments. In this work, signal normalization to bulk constituents was used and an internal standard was defined for all measurements of solid samples in order to overcome those aberrations.

To illustrate how scan speed impacts measurement accuracy a calibration function for hydrogen sintered samples of different boron contents was set up and is presented in Figure 44. Iron (^{58}Fe signal marked with a green line) was defined as the internal standard for all measurements performed throughout this present work since its signal is nearly constant in time and it is present in high amounts in each investigated sample (same for ^{53}Cr and ^{85}Mo). As mentioned before, ^{11}B/^{58}Fe as a normalized signal was used for boron quantification in order to provide reproducible measurements which are independent of equipment aberrations (inconsistency in gas flow, ionization, measurement drifts, etc.).
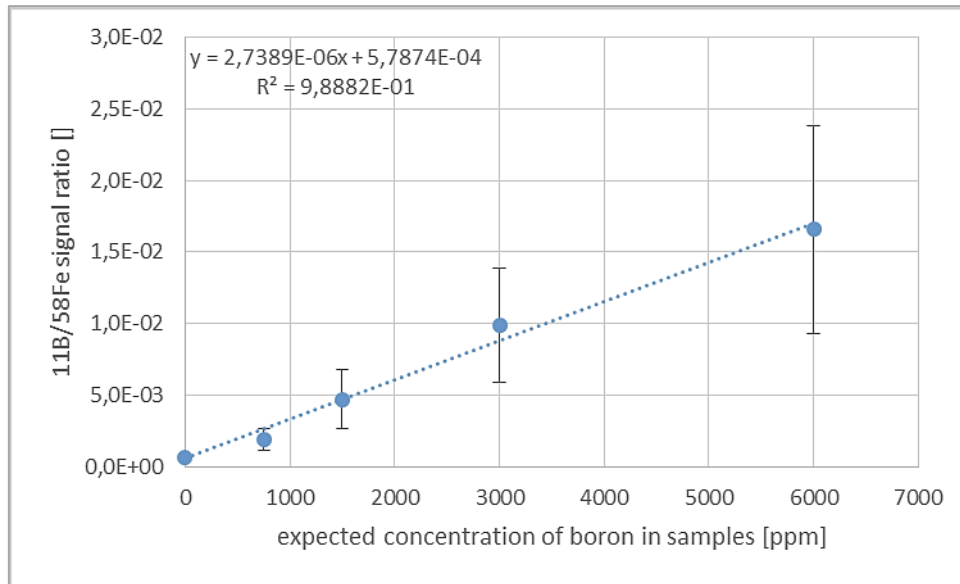
Figure 44 - calibration function of hydrogen sintered samples of different boron concentrations; normalized signal is the average value of 5 line scans per sample (10 Hz, 200 μm spot size, 100 μm/s scan speed, 5.71 J/cm², 0.5 l/min gas flow, 4mm² investigated area)

Signal ratios for each sample were calculated according to 2.6.2. First, average signal ratio of each region was determined. Then the average of six regions (corresponds to one line scan) was calculated. Finally, the average signal ratio of all five line scans was established and plotted in Figure 44. Average standard deviation which is illustrated graphically in Figure 44 characterizes the deviations in signal ratio of each sample and is calculated among those 5 line scans. Due to all the negative effects associated with slow scan speed points of measurement are quasi interchangeable since standard deviations of neighboring points overlap. Moreover, the size of the investigated sample area (4mm²) is not large enough, to provide a representative analysis.

Considering the previous issues, there was a need for optimization towards higher scan speed and larger areas of ablation in order to provide representative and reproducible measurements for a valid quantification of boron in argon and hydrogen sintered samples. So as to do so, a method for the quantification of boron in solid standards needed to be established.

Optimum parameters for measuring boron concentration in solid standards sintered in vacuum were determined and are presented in Table 9. Increasing scan speed to 300 μm/s led to more consistent analyte signal paths during measurement while at the same time providing more representative and reproducible measurements by enhancing the area of investigation to about 14.5 mm². The improvements achieved can be obviously identified in Figure 45.
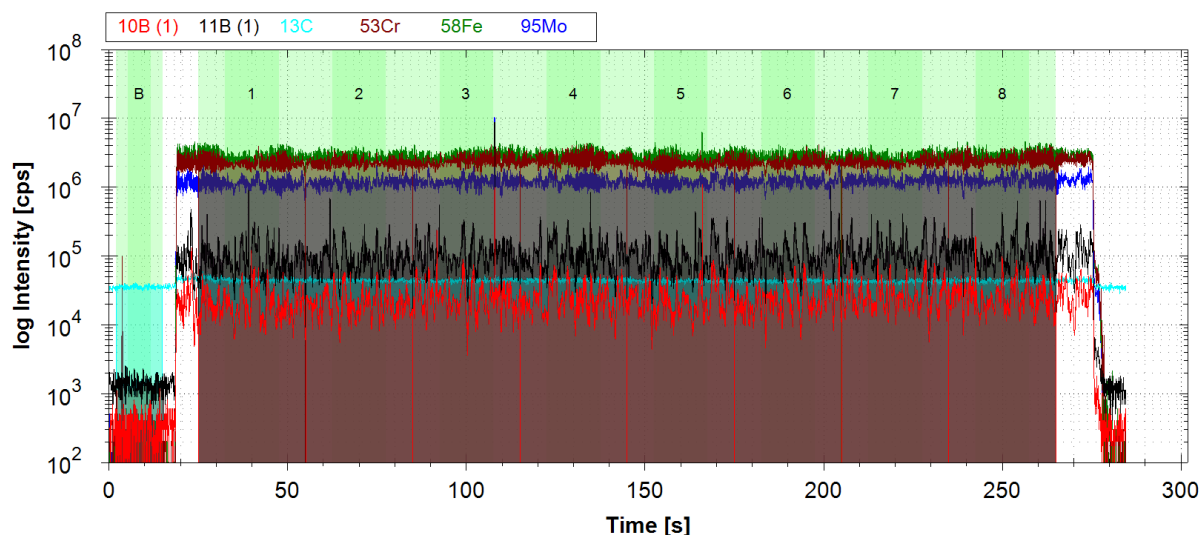
Figure 45 - example of a line scan of 3000ppm vacuum standard with increased scan speed (300 μm/s) showing improvement in signal consistency (10Hz, 200μm spot size, 5.71 J/cm², 0.5 l/min gas flow, 14.5mm² investigated area)

One can tell that boron signal is much smoother during measurements. This is due to the fact that the laser spends less time per ablated area so that changes in signal happen much faster and more sudden. Therefore the periodic change of ^{10}B and ^{11}B signal is much more uniform. Also, it was determined that increasing the measuring time results in improvements of the uniformity and consistency of the analyte signal during analysis. By doing so, the analyte signal becomes less susceptible for outliers and artifacts. Applied to the circumstances of this current work, inconsistencies in sample uniformity do not affect average signal calculations that significantly. Hence, the measuring time was increased and set to 4min per line scan (20 min per sample).

The calculated average intensity of the two boron isotopes is much more accurate and precise as expected. As it can be seen from the following figure (Figure 46), the square root of the sample correlation coefficient indicates that the calibration function of solid standards matches well with the measured average normalized signals of solid standards. Moreover, standard deviation of that signal is highly improved so that the measured neighboring points are not interchangeable anymore.

Another important factor was the adjustment of the carrier gas flow (He). An optimization of said parameter was crucial since high retention time of ablated particles in the ablation chamber can lead to intense peak broadening. Gas flow rate was set to be 0.5 L/min for all LA-ICP-MS experiments performed on solid samples.

Now, with the successful quantification of boron in vacuum sintered solid standards via liquid measurements (3.3.1), the calculated concentrations could be assigned to those specimen. Table 21 provides a comprehensive overview of that data.

Table 21 - calculated concentration of boron in vacuum sintered solid standards using calibration function in Figure 42

Sample name	Calc. conc. [ppm]	Average ^{11}B/^{58}Fe	STDEV ^{11}B/^{58}Fe	RSD [%]
0-vac	0	1.85E-03	4.55E-04	25
1500-vac	1138	2.84E-02	1.74E-03	6.1
3000-vac	2118	4.97E-02	3.08E-03	6.2
6000-vac	5479	1.15E-01	4.68E-03	4.1
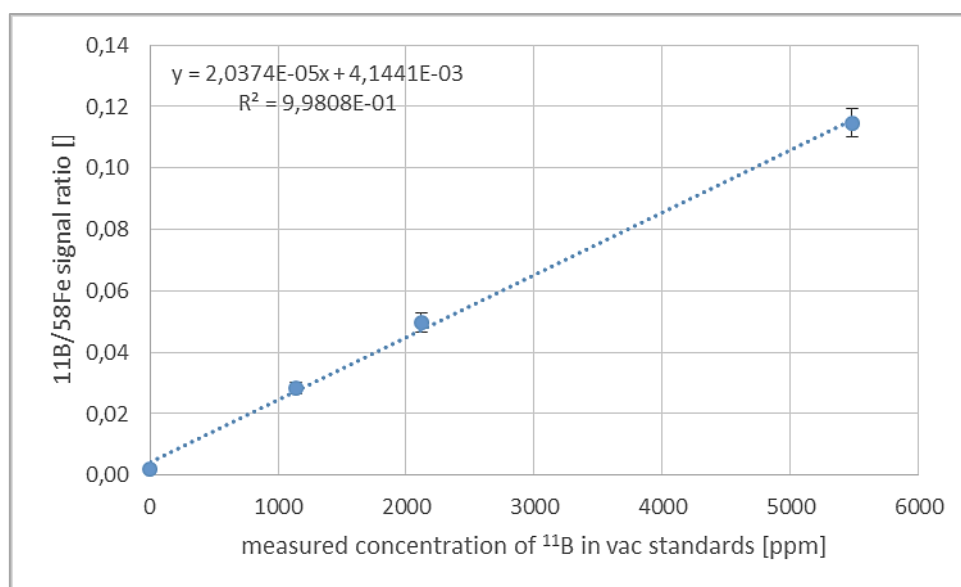
Figure 46 - concentration of boron (^{11}B) in vacuum sintered samples calculated with the calibration function of Figure 42 (10Hz, 200μm spot size, 5.71 J/cm^2, 0.5 l/min gas flow, 14.5mm^2 investigated area/line scan)

Finally, a functioning method for the quantification of boron in solid samples via LA-ICP-MS was established and performance enhancing adjustments were carried out leading to the desired calibration function, which enables quantifications of boron in argon and hydrogen sintered samples. Furthermore it has to be pointed out that after reviewing results for the solid standard 750-vac, it was decided to exclude said data from further calculations. Unexpected problems with sample preparation, especially during powder mixing, lead to extensive inhomogeneity of constituents in the sintered sample, resulting in high deviation and the loss of reproducibility. With this method a limit of detection of 179 ppm for ^{11}B could be achieved. Adjustments concerning the LOD could definitely be made by increasing purging

time of the ablation chamber. However, considering the high quantities of boron which are present in the investigated samples, limits of detection are satisfying for the task of the present work.

3.3.3. Measurement of Total Boron Concentration in Argon and Hydrogen Sintered Samples

Determination of the total boron concentration in argon and hydrogen sintered samples was carried out exactly according to 2.6.2. Laser parameters were set to be 10Hz laser pulse frequency, 200µm spot size, 5.71 J/cm² fluency, 0.5 l/min helium gas flow and resulting in an investigated area of 14.5mm². Considering the adjusted measurement parameters, the signal intensity for ^{11}B was sufficient and located in a range of 10^5-10^6 cps (logarithmic intensity) during measurement. The background signal for ^{11}B was accounting for about 10^3 cps maximum. That being said, in terms of signal output, trouble-free LA-ICP-MS measurement of argon and hydrogen sintered samples was ensured.

3.3.3.1.   Argon Sintered Samples

Measurement results are presented graphically in Figure 47.
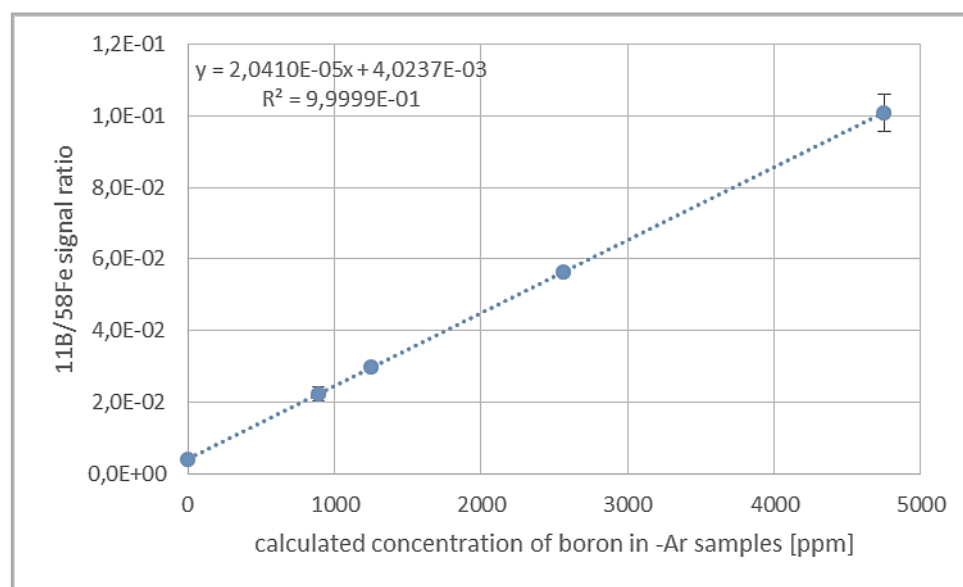
Figure 47 - fitting function for normalized ^{11}B signal of Ar sintered samples plotted against calculated concentration of boron (10Hz, 200µm spot size, 5.71 J/cm², 0.5 l/min gas flow, 14.5mm² investigated area/line scan)

The boron concentration in the investigated samples was evaluated and is shown in Table 22. The calibration function of vacuum sintered solid standards was used for calculations.

Table 22 - calculated concentration of boron in Ar sintered samples; calibration function: y = 2,0374E-05x + 4,1441E-03

Sample name	Cal. conc. [ppm]	STDEV [ppm]	RSD [%]
750-Ar	892	78	8.8
1500-Ar	1252	41	3.3
3000-Ar	2565	28	1.1
6000-Ar	4751	245	5.2

3.3.3.2.   Hydrogen Sintered Samples

The same measurements and calculations were performed on hydrogen sintered samples, differing in their boron contents. They are presented in the following (Figure 48 and Table 23).
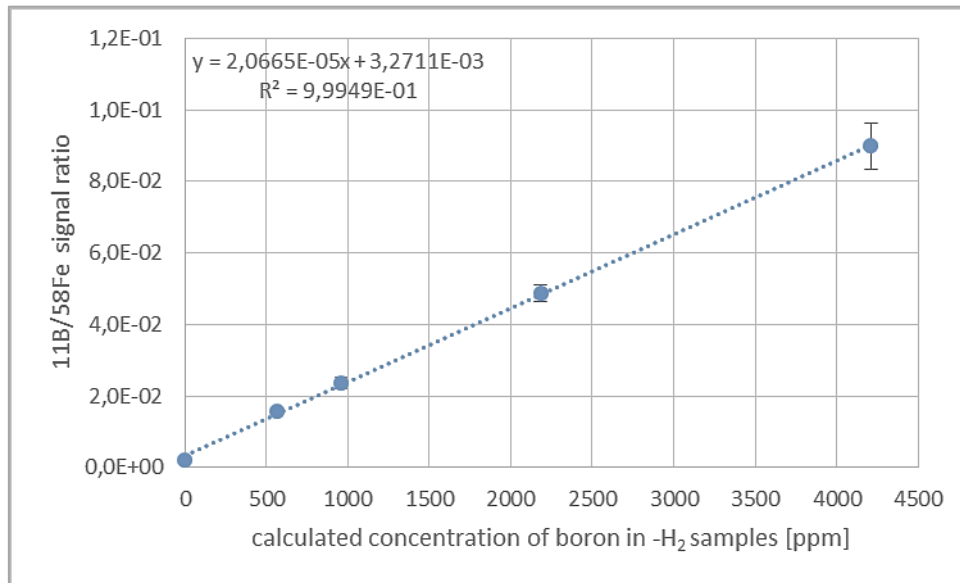
Figure 48 - fitting function for normalized ^{11}B signal of H_2 sintered samples plotted against calculated concentration of boron (10Hz, 200µm spot size, 5.71 J/cm², 0.5 l/min gas flow, 14.5mm² investigated area/line scan)

Table 23 - calculated concentration of boron in H_2 sintered samples; calibration function: y = 2,0374E-05x + 4,1441E-03

Sample name	Cal. conc. [ppm]	STDEV [ppm]	RSD [%]
750-H2	565	32	5.7
1500-H2	960	62	8.9
3000-H2	2183	106	4.9
6000-H2	4211	301	7.1

Based on the calibration functions for both argon and hydrogen sintered samples, satisfying accuracy and precision of results could be achieved. The inconsistency of the boron signal caused by the lack of uniformity of boron in those specific samples due to grain boundary segregation, gas inclusions and mixing inefficiency (mentioned in 3.3.2) reflecting the inconsistency of the boron signal, could finally be overcome by optimizing laser parameters and increasing scan speed. Results for the boron concentration of samples sintered in in all three atmospheres are depicted in Figure 49. Calculations were carried out using the calibration function for solid standards (vacuum sintered).
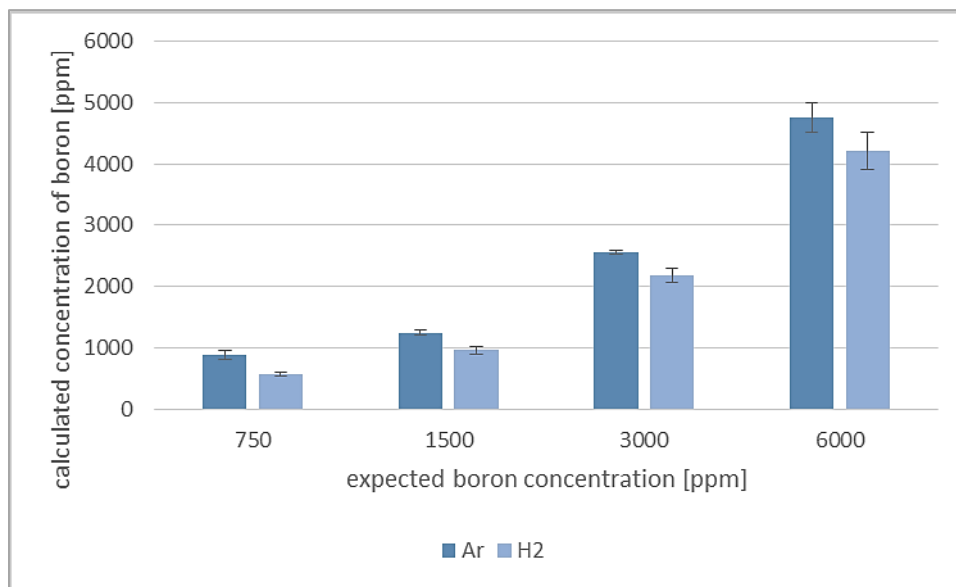
Figure 49 - comparison of calculated boron concentration in Ar and H₂ sintered specimen

Concerning vacuum sintered solid standards, it has to be pointed out that calibration was set up based on four data points which means that results for the standard 750-vac where excluded (more in chapter 3.3.2). First of all, results for boron concentration indicate differences when comparing the expected concentration to the calculated one. More precisely, the calculated concentration is lower than the expected one, without any exceptions. Reasons for this discrepancy could lie in systematic errors occurring during preparation of standards (dilution process) or when weighing in powders. Other than that, difficulties during powder mixing, namely the formation of agglomerates and segregation leading to the loss of uniformity, are major sources of errors and have been discussed before. On top of that, it must be emphasized that for each sample of a specific boron content and sintering gas, only one specimen has been manufactured. Hence, results are based on multiple measurements of only one and the same sample and, therefore, they are directly bound to the characteristics of that particular specimen. Consequently, there is more or less no

statistical evidence for the validity of those single results which means that there is a possibility for them to be outliers thus being non-representative.

Regarding the entirety of all those mentioned sources of errors, no greater importance should be attached to the results for calculated concentration of boron in Table 21 and in Figure 46, because those of argon and hydrogen sintered samples are directly linked to, even derive from, calculations based on the determination of the boron content in vacuum sintered samples via liquid measurements.

Speaking about vacuum sintered samples, they were awaited to show the highest concentrations of boron since no loss of the analyte was anticipated during sintering (as it is expected to happen for hydrogen and probably even for argon sintered samples). However, solid standards do not exhibit the highest contents of boron except sample 6000-vac which exceeds boron concentrations of hydrogen and argon sintered samples by about 20%. Again, previously discussed facts have to be considered for interpretation.

Comparing argon and hydrogen sintered samples, results suggest lower concentrations of boron for the latter. That being considered, a reasonable argument for the loss of boron in hydrogen sintered samples can be made.

However, considering the set-up of a calibration function for solid measurements (besides achieving low standard deviation of the mean value (≤8%) for all data points), the method development for the quantification of boron in bulk material, in terms of parameter adjustments, has been successfully accomplished. With other words, the accuracy and precision of results is given within one sample (n=1). The processing and analysis of PM-steel sample replicates via LA-ICP-MS is the key-factor for data validation and statistical assurance.

3.3.4. Measurement of Depth Profile of Boron in Argon and Hydrogen Sintered Samples

Literature suggests that boron reacts with hydrogen gas, forming volatile hydro borides when sintering in hydrogen atmosphere[55]. Therefore, boron content in hydrogen sintered samples is expected to be lower than in those sintered in argon atmosphere. As mentioned in the previous paragraph and illustrated in Figure 49, results from measurements of total boron concentration confirm said claim.

---

[55] (Selecka & Bures, Metallography 1998, 1998)

The sample surface constitutes an interface which is in constant interaction with its surrounding atmosphere. In this particular case the chemical interaction between the hydrogen gas and the sample surface is of major importance when talking about the formation of volatile hydro borides. Since the mentioned interaction is most intense at that interface, a loss of boron is expected to be the greatest at the surface and adjacent areas. Hence, there should be differences in boron concentration when comparing surface and bulk material (deeper areas).

In order to investigate on that particular behavior a method for the quantification of boron in terms of creating a depth profile was established. Measurements were performed on LA-ICP-MS according to 2.6.4. and samples 3000-Ar and 3000-H2 were investigated. Figure 50 provides a schematic arrangement for the LA-ICP-MS boron depth-profile measurements.
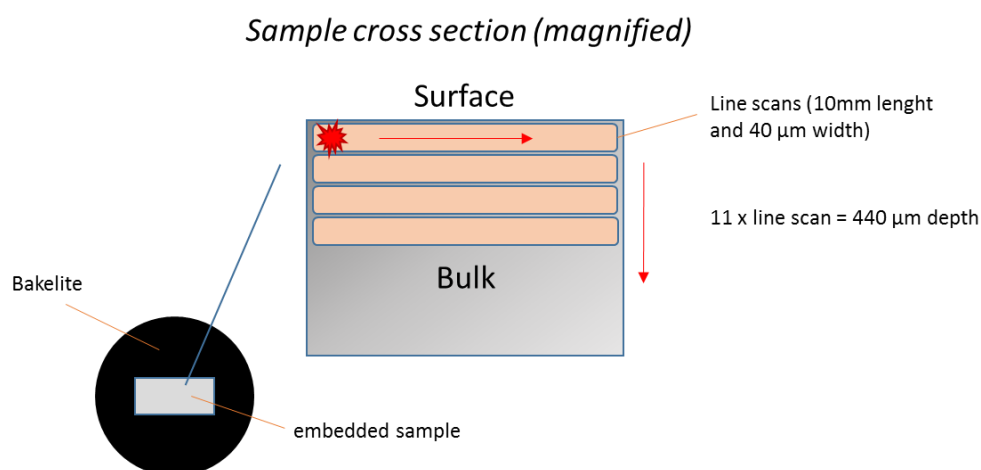
Figure 50 - schematic set up of LA-ICP-MS boron depth profile measurement

In Figure 51 and Figure 52, the normalized boron signal is plotted against sample depth and illustrated. For the following graphs, each point of measurement represents the average value for the particular signal ratio of each line scan and its standard deviation calculated according to 2.6.4.
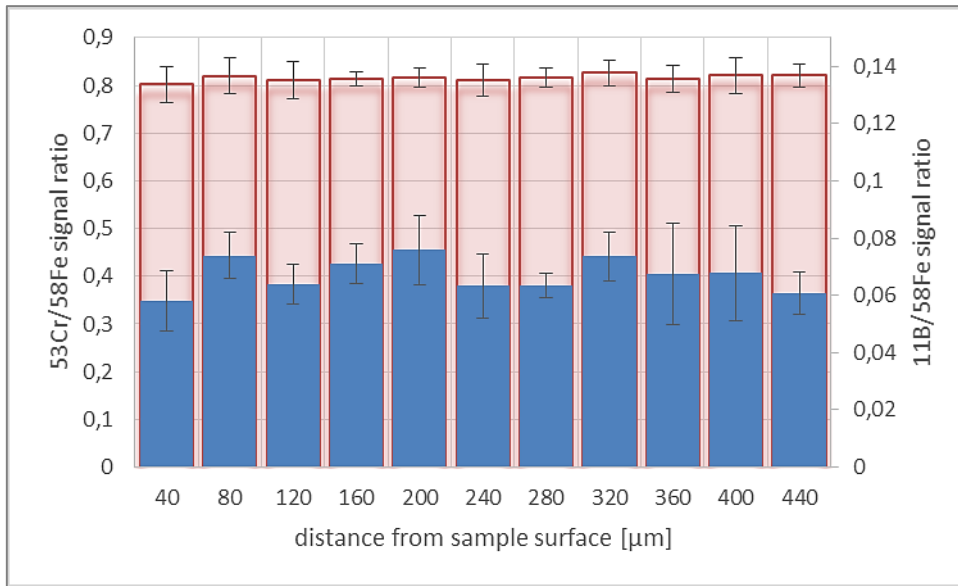
Figure 51 - 11B/58Fe signal ratio (blue column) depending on sample depth of argon sintered samples (3000-Ar). 53Cr/58Fe signal ratio (red column) is constant through sample depth.
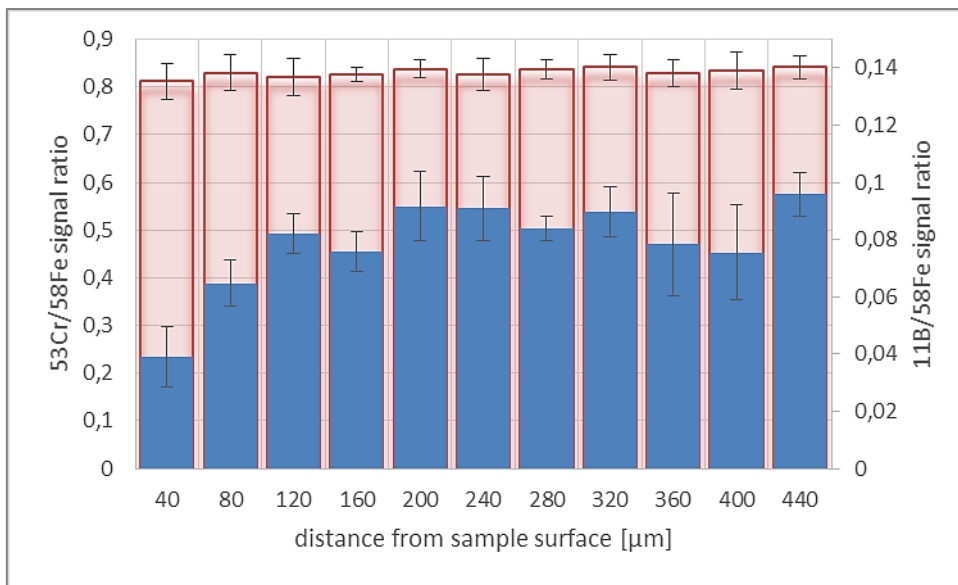
Figure 52- 11B/58Fe signal ratio (blue column) depending on sample depth of hydrogen sintered samples (3000-H2). 53Cr/58Fe signal ratio (red column) is constant through sample depth.

Indeed, results in Figure 52 suggest a lower normalized boron signal at surface adjacent areas compared to those in the bulk material. In fact, a concentration gradient is to be pointed out for the hydrogen sintered sample. For the sample which was sintered in argon atmosphere however, there is no such gradient to determine.

In order to show the consistency in signal development of both ^{58}Fe and ^{53}Cr throughout the recording time, the signal ratio of those isotopes is shown in Figure 51 and Figure 52, whereas standard deviation of the average of all points of measurements is evaluated as about 1%.

64

Those results validate the investigated boron concentration gradient by showing that only the ^{11}B signal contributes to the differences in signal ratio with respect to the sample's depth and not the signal of the internal standard, as it is proven to be consistent during measurements.

Nevertheless, this measuring method has its limitations: With a scan time of about 2 minutes per line, which accounts for an area of investigation (ablation area) of about 2.1 mm^2 with present laser settings (Table 11), the amount of recorded data is not sufficient enough for representative calculations. Also, since there is an expectation for a non-homogenous distribution of boron in the samples, not only for ablation in a lateral manner but also in depth, the latter should be held to a minimum to ensure the reproducibility of measurements. Therefore, the stacking of line scans (repeating a line scan at the same location on the sample) would lead to a line crater of an inestimable depth and should be avoided. Considering the latter facts, the maximum achievable of the ablated area for one line scan (resolution of 40μm) is limited to the sample width.

In order to increase the area of ablation, hence to assure representative and reproducible measurements, four line scans each with a size of 14.5 mm^2 were performed on sample surfaces and cross sections of both argon and hydrogen sintered PM-steel specimen. Parameters for that particular LA-ICP-MS analysis method can be seen in Table 12. This method enabled a quantification of boron in bulk material compared to the sample surface. Results are presented in Figure 53. For samples sintered with hydrogen, lower normalized boron signals can be examined at the surface compared to sample bulk, especially for samples containing higher amounts of boron (3000-H2). Then again, argon sintered samples do not show any differences in that regard. It can be argued that concentration of boron does not change significantly within the sample. Considering the remarkable reproducibility of the experiment expressed by low standard deviation (≤ 8%), a reasonable argument can be made for the existence of a boron gradient in the outermost, surface adjacent areas of the hydrogen sintered samples, as well as its inexistence in argon sintered specimen, as stated by the results in Figure 51 and Figure 52. Once again, it has to be emphasized that results are based on the measurements of only one specimen per sample. With all the limitations being considered in terms of sample reproducibility which were discussed in 3.3.3, there is a need for the production and measurement of sample replicates in order to validate those results and assure statistical proof.
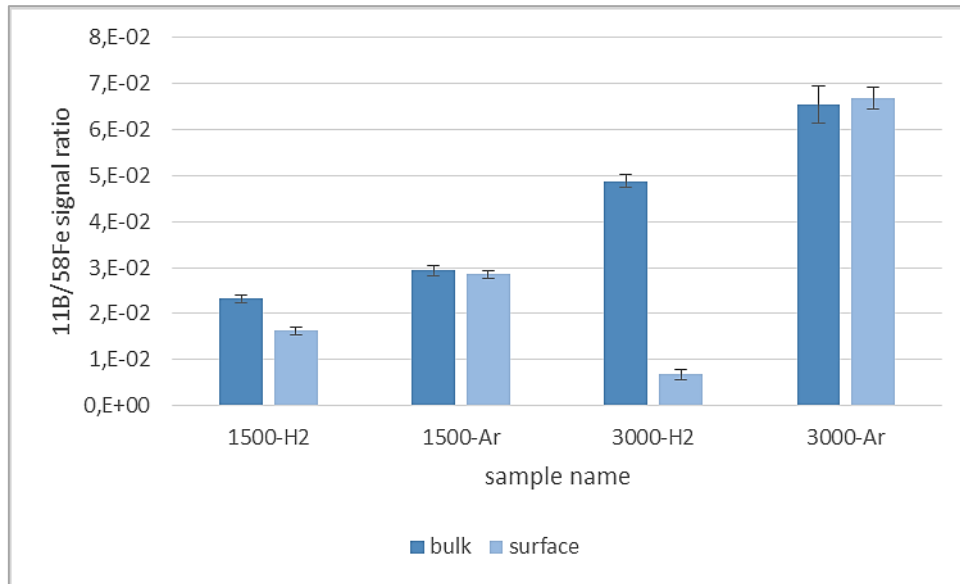
Figure 53 - 11B/58 Fe signal ratios measured at sample surface and bulk of argon and hydrogen sintered samples (10Hz, 200μm spot size, 5.71 J/cm², 0.5 l/min gas flow, 14.5mm² investigated area)

Finally, attention has to be drawn to the interpretation of the results provided by these measurements in order to not make inappropriate statements. For the results provided in Figure 51 and Figure 52, the resolution of the local boron signal is dependent on the laser spot diameter which would be 40 μm for this particular method of measurement. That being said, the local ^{11}B signal in this area is resolution-bound, meaning that those signals for the randomly chosen points A and B within the laser diameter are not distinguishable. Referring to the results conducted via the established method for the in depth quantification of boron, points of measurement in the presented figures represent the average signal ratios with a vertical length of 40 μm. Therefore, it is important to keep in mind that results give proof of the existence of a boron concentration gradient in hydrogen sintered samples, but the calculated signal ratios (points of measurement) are always average values and their resolution is limited to the laser spot diameter.

Of course, resolution can be improved by decreasing the laser spot diameter, however, the loss of signal intensity (in cps) has to be taken into account. The boron background signal is the limiting factor for this method and has to be considered when optimizing the measurement resolution. Also, sample geometry turned out to be not perfectly rectangular especially for specimen containing higher amounts of boron (3000 and 6000ppm samples, respectively) which posed difficulties for the line scan alignment since ablation lines could not be fitted perfectly to the crooked sample surface (resulting in altering line scan-sample surface

distances). These circumstances contribute to the accuracy and precision of that measuring method.

3.3.5. Measurement of Lateral Boron Concentration in Ar and H_2 Sintered Samples

Elemental mapping of boron, which is also known as imaging, was carried out according to 2.6.3. Laser parameters can be found in Table 10. The measurements were performed on samples 3000-Ar and 3000-H2, respectively. Results are presented in Figure 54 and Figure 55 in the following. Each of those show an image of the boron distribution (left) and a picture of the investigated area (right) of the particular sample.
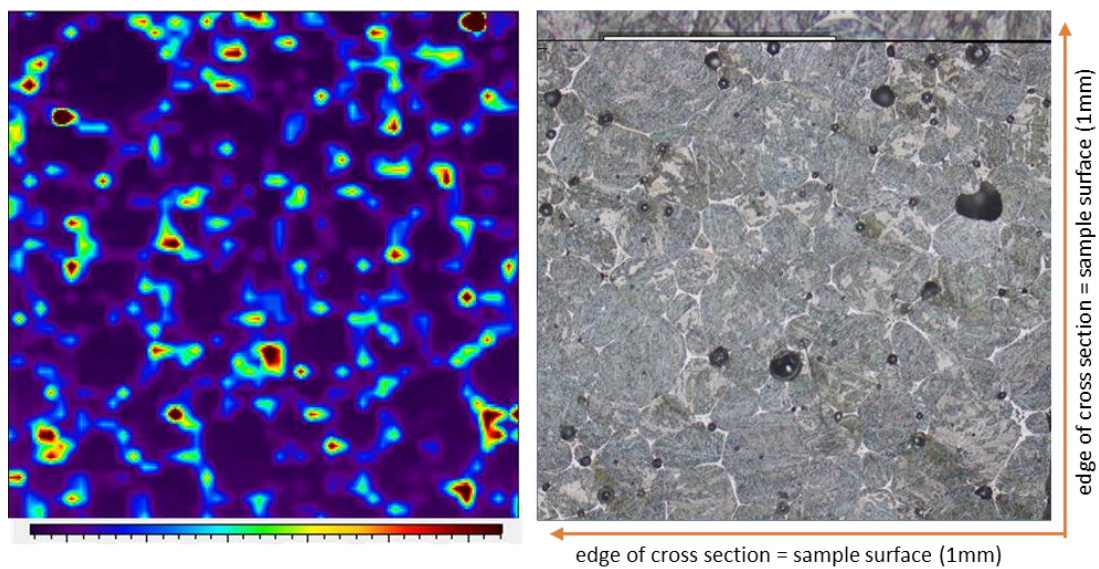
Figure 54 - distribution of boron (^{11}B normalized on iron) in an area of $1mm^2$ of the sample 3000-Ar (left) and its belonging microscopic image (right)
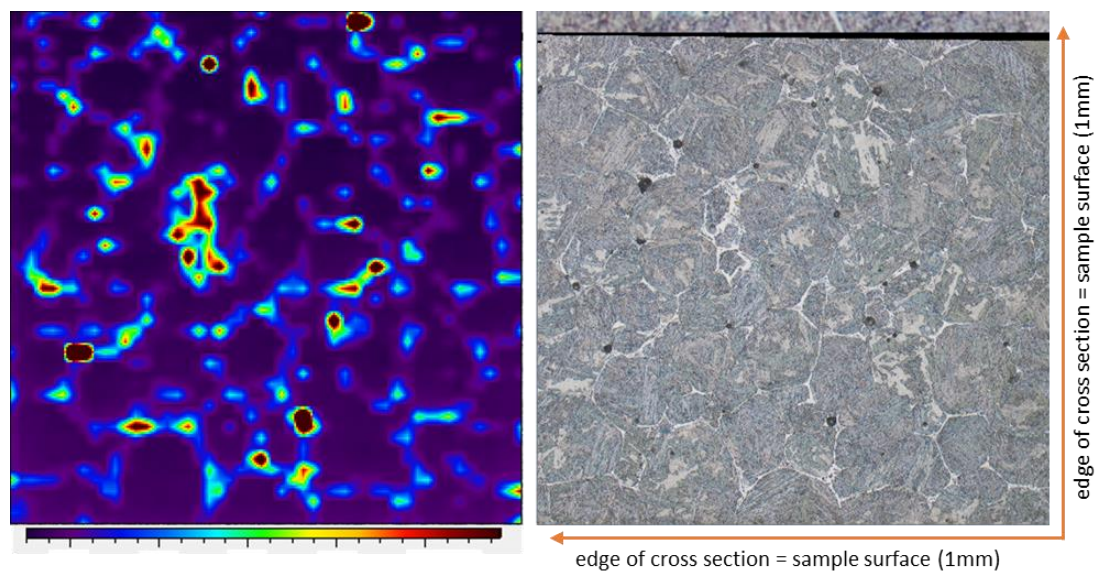
Figure 55 - distribution of boron (^{11}B normalized on iron) in an area of $1mm^2$ of the sample 3000-H2 (left) and its belonging microscopic image (right)

The bottom right of the picture represents the edge of the sample (taking into account the direction of orange arrows in Figure 54 and Figure 55). The ablated area of each figure has a size of 1x1 mm with a lateral resolution of 20 μm. This means that for every pixel the average signal is calculated and assigned to it. For this particular imaging process a method has been developed which enables the calculation of the average of the normalized ^{11}B signal (^{11}B/^{58}Fe). Each pixel is represented by a specific color which is dependent on the intensity of that average signal ratio. The applied color scale, consisting of a gradient from dark blue (lowest ^{11}B/^{58}Fe signal) to bright red (highest), is attached to the images above.

That being said, it is important to point out that this kind of quantification only describes the local boron concentration but it does not provide information about the total concentration of boron in the sample. After all, it does provide an overview of the distribution of boron in the investigated area.

All in all, the imaging of boron matches perfectly with the locations where major amounts of boron were expected to be found (white areas consisting of boron a rich, solidified eutectic phase). Also, one can argue that the surface areas of the samples which were sintered with hydrogen gas, contain smaller amounts of boron compared to the ones sintered with argon, supporting the argument that boron is forming volatile hydro borides with hydrogen gas during sintering. Moreover, when looking at Figure 54 and Figure 55 respectively and assuming that the investigated area is representative of the whole sample, one can make a legitimate argument that sample 3000-Ar exhibits a higher amount of boron than in sample 3000-H2 which would support the results shown in Figure 49, stating that all samples which where sintered with hydrogen gas suffer from a significant loss of boron. Finally, is interesting to see, that although there are also some residues of former liquid phase on the edge of the sample sintered in hydrogen, the boron is much more evenly distributed in the sample sintered in argon.

4. Conclusion and Outlook

The objective of this work was to develop and establish a method which enables the quantification of boron in PM-steel-samples via LA-ICP-MS. Further goals were to investigate on the effect of argon and hydrogen as sintering gases on the boron content of those samples as well as to establish a better understanding of the impact of that element on the specimen properties.

First of all, a measuring method for the quantification of boron in solid samples via LA-ICP-MS was developed, resulting in a successful set up of a calibration function for the $^{11}B/^{58}Fe$ signal ratio, when using ^{58}Fe as an internal standard. In order to achieve this, self-made, vacuum sintered solid standards were processed with a decent uniformity of constituents, although the manufacturing of such standards was a difficult task, since homogenous distribution of the analyte in the steel matrix had to be provided. Also, the analysis of aqueous standards and digested vacuum samples had to be performed initially on the ICP-MS in order to evaluate the analyte concentration. Finally, LA-ICP-MS analysis of vacuum sintered solid standards resulted in a linear slope with a LOD of 179ppm and 8% standard deviation of mean.

With that preliminary work invested, different approaches for the quantification of boron (total concentration, lateral distribution and in-depth quantification) in argon and hydrogen sintered samples were tested. For each one, measuring methods were established by optimizing laser parameters and sample preparation. Doing so enabled making certain claims associated with boron in PM-steel-samples.

The quantification of the total concentration of boron via LA-ICP-MS could be carried out for both argon and hydrogen sintered steel samples. Calculations were performed on the basis of the regression function for vacuum sintered solid standards. Regarding those results, which indicate lower concentration of boron in hydrogen sintered samples with respect to the samples sintered with argon, it can be claimed that there is a significant loss of boron taking place during sintering, arguably due to the formation of hydro borides.

Second, a method for the evaluation of the distribution profile of boron using line scans was established. For that matter, sample cross sections were scanned from the surface towards sample center. Concerning hydrogen sintered samples, a concentration gradient for boron in the surface adjacent layers (≤100 μm approx.) could be pointed out whereas concentration does not show significant changes in argon sintered samples. Further, the concentration of

boron on the sample surface and in the bulk material was determined and compared to each other, again indicating high loss of boron at the surface in hydrogen sintered samples.

Finally, Imaging of sample cross sections was carried out in order to determine the lateral distribution of boron. Images revealed boron-rich phases and emphasized a much less uniform distribution of boron in argon sintered samples.

Another point of emphasis was to investigate in the physical and mechanical properties. Also metallographic examinations were carried out. Taken into account all the results provided by LA-ICP-MS analysis, a correlation between investigated material properties and boron concentration in samples was established. Densification enhances with increasing boron content which could be determined and localized via LA-ICP-MS measurements at the grain boundaries, solidified as a eutectic, boron-rich phase. Moreover, the quantities of the analytically detected boron match with the observations of harder and more brittle materials with increasing boron contents.

In general, LA-ICP-MS has turned out to be a promising method for the quantification of boron in PM-steel. The ability of a quasi-non-destructive, basically non-sample-preparative (for solid samples) measurement makes it a fast analysis tool with a low sample consumption. Moreover, the isotope analysis of boron benefits from the fact that it is free of elemental interference, facilitating the measurement and evaluation process as well as preventing signal loss. Also, multielement analysis of main constituents Fe, Cr and Mo allowed determination of ^{58}Fe as an internal standard which enabled reproducible measurements. The LA-ICP-MS measurement of solid samples requires matrix matched calibration standards, since the ablation process is strongly matrix dependent, which is also the downside of that instrument. Most definitely, the absence of certified standard materials posed a limitation to the reproducibility of the experiments. The manufacturing of such standards was a difficult task, since homogenous distribution of the analyte in the steel matrix had to be provided. Therefore fabrication of standards with known boron contents is essential for the success of the method.

First steps towards the development of a reliable method for the quantification of boron in PM-steel have been successfully taken. At the same time, there is a lot of work left for further optimization. Homogeneity of components in self-made solid standards is still a factor of inconsistency and processing steps of standard preparation (powder mixing and sintering) are poorly investigated, hence they can potentially be improved. Most importantly, replicates of

the investigated samples need to be processed and analyzed in order to validate the obtained results and achieve statistical security.

Depth-profile analysis of boron can be optimized as well. Up to this point, a minimum spot size of 40µm for line scans could be achieved resolution wise whilst assuring sufficient signal for analysis. However, improvements in imaging (lateral quantification) and analysis of depth profile of boron in terms of spatial resolution are mostly limited to the inhomogeneous distribution of boron in investigated solid samples. Therefore, either sample preparation needs to be enhanced or certified standard material to be acquired to establish sufficient local resolution of boron.

Talking about the evaluation of the total concentration of boron in samples, the manufacturing of thin sample slices, for instance with a cutting tool such as a focused ion beam (FIB), would mean great improvements of results provided by LA-ICP-MS analysis in terms of representation and accuracy, since the contribution of errors originating from the vertical distribution of boron would be decreased.

Lastly, in relation to this current work, it must be emphasized that for each sample of a specific boron content and sintering gas, only one specimen has been manufactured. Hence, results are based on multiple measurements of only one and the same sample, meaning that magnitudes of errors originating from sample specifics can neither be ignored nor calculated. That being said, one has to be aware that results gained throughout this work can, but most definitely do not have to be necessarily limited on the samples presented here. In order to be able to deliver more general and representative results and statements, replicates of all sample specimen have to be investigated.

Literaturverzeichnis

ASTM. (2012, 11 09). *www.astm.org*. Retrieved from www.astm.org/.../B09%20Final%20Version%20of%20Revised%20Gray...

Bendereva, E., & Vylkanov, S. (2012). ACTIVATING EFFECT OF BORON MICROADDITIONS ON SINTERING OF POWDER ALLOY BASED ON IRON. *Metallurgist, vol. 55*, p. 761.

Benesovsky, F., Hotop, F., & W.Frehn, F. (1955). *Planseeber. Pulvermetallurgie, vol.3*, p. 57.

Bonta, M. (2013). *Elemental imiging using LA-ICP-MS on biological samples.* Vienna: TU Vienna.

Brown, P., & Hu, H. (1996). *Ann. Bot.*, p. 77.

Corti, C. (1986). Sintering Aids in Powder Metallurgy. *Platinum Metals Review vol. 30*, pp. 184-195.

Crowson, A., & Burlingame, J. (1982). *Processing of Metal and Ceramic Powders*, pp. 199-211.

Eaton, A., & Franson, M. (2005). *Standard Methods for the Examination of Water & Wastewater.* Amer Public Health Assn.

Fernandez. (2007). *Tr. Anal. Chem.*

German, R. (1983). *Int. J. Powder Metall. & Powder Technol., vol. 19, no. 4* , pp. 277-287.

German, R., & Munir, Z. (1982). *Reviews Powder Met. Phys. Ceram.*, pp. 9-44.

German, R., & Rabin, B. (1985). *Powder Metall. 28*, p. 7.

Gierl, C., Moshin, U., & Danninger, H. (2008). *Powder Metallurgy Progress; Vol. 8; No 2.*, p. 135.

Graphit Kropfmuehl/AMG Mining AG. (2013, 07). *www.gk-graphite.com.* Retrieved from http://www.gk-graphite.com/uploads/media/Friction_02.pdf

Günther, & Hattendorf. (2005). *Trends in Analytical Chemistry, Vol. 24, No. 3*, p. 256.

Höganäs AB. (2013, June). *hoganas.com*. Retrieved from www.hoganas.com/pmc

Houdremont, E. (1956). *Handbuch der Sonderstahlkunde.* Düsseldorf: Verlag Stahleisen m.b.H. .

Houdremont, E. (1966). Special Steels vol 1 and 2 [Russian Translation]. *Metallurgiya*.

IUPAC. (1998). Isotopic Compositions of the Elements. *Pure and Applied Chemistry vol. 70*, p. 217.

Kazior, J. (2002). The influence of boron on the mechanical properties of prealloyed. *Deformation and Fracture in Structural PM Materials, vol.1*, pp. 125-131.

Key to Metals AG. (2007, November). Retrieved from www.totalmateria.com: http://www.totalmateria.com/page.aspx?ID=CheckArticle&site=kts&NM=212

Koch, J., & Günther, D. (2011, 02 11). Review of the state-of-the-art of laser ablation inductively coupled plasma mass spectroscopy . *Applied Spectroscopy*, pp. 155-162.

Ludwig, E. (2014). *Development of ICP-based methods for quantification of sulfur in electro-deposited copper samples.* Wien.

Madan, D. (1991). *Int. J. Powder Metall. vol 27*, p. 339.

Madan, D., German, R., & James, W. (1986). *Progr. Powder Metallurgy vol. 42*, p. 267.

Mokgalaka, & Gordea-Torresdey. (2006). *Applied Spectroscopy Reviews, Vol 41*, p. 132.

NDT resource center. (2015, 03 03). *NDT resource center*. Retrieved from www.nde-ed.org

Nischkauer, W. (2011). *Development of advanced methods for the determination of Platinum Group Elements in plant material.* Vienna: TU Vienna.

Rao, R., Parab, A., Sasibhushan, K., & Aggarwal, S. (2009). A robust methodology for high precision isotopic analysis of boron by thermal ionization mass spectrometry using Na2BO2+ ion. *Int. J. Mass spectrom vol. 285*, pp. 120-125.

Röttger, A., Weber, S., & Theisen, W. (2012). *Materials Science and Engineering A, vol. 532*, pp. 511-521.

Sah, R., & Brown, P. (1997). Boron determination - a review of analytical methods. *Microchem. J. vol. 56*, pp. 285-304.

Schade, C., Schaberl, J., Thakur, S., & Dongre, V. (2005). *Pre-alloyed boron in powder metal (P/M) stainless steel.*

Selecka, M., & Bures, R. (1998). Metallography 1998., (p. 122).

Selecka, M., Salak, A., & Danninger, H. (2003). *Journal of Mat. Processing Technology, vol. 141*, pp. 379-384.

Thomas, R. (2001, 10). A Beginner's guide to ICP-MS, Part VI- The Mass Analyser. *Spectroscopy*.

Vassileva, V., Danninger, H., & Gierl, C. (2007). *Proc. Euro PM2007; European Powder Metallurgy Association; Vol. 1*, p. 53.

wikipedia.org. (2004, 07 20). Retrieved from http://upload.wikimedia.org/wikipedia/commons/3/3d/ICP-Brennerduese.png

Wright, C., Fryer, F., & Woods, G. (2008). Rinse Solution for Boron Analysis and Boron Isotope Ratios. *Agilent ICP-MS Journal, vol. 33*, 4-5.

www.slideshare.net. (2014, 09 29). Retrieved from http://image.slidesharecdn.com/masspart2-140929003457-phpapp02/95/mass-part-2-25-638.jpg?cb=1411969049

Yoshitomi, K., Nakama, Y., Ohtani, H., & Hasebe, M. (2008). *ISIJ Int., vol 48*, pp. 835-844.

Zhang, G., Li, J., Wei, S., & Zhao, Q. (2011). *Applied Mechanics and Materials, vol. 52-54*, pp. 1718-1722.

Zovas, P., & German, R. (1983). *J. Metals, vol. 35*, pp. 28-33.

List of Figures

List of Tables

List of Equations